Minimum-Time Trajectories of Electric Sail with Advanced Thrust Model

Alessandro A. Quarta [1], Giovanni Mengali [2],

Dipartimento di Ingegneria Civile e Industriale, University of Pisa, Italy

Abstract

The Electric Solar Wind Sail is an advanced propulsion system concept that, similar to the more conventional solar sail, is able to generate a propulsive thrust without any propellant. The main performances of such a propulsion system have been studied in different mission scenarios and are reported in the literature. However, the analyses available so far are based on a simplified thrust model that neglects the effect of the spacecraft attitude on both the thrust modulus and its direction. The recent availability of a refined thrust model requires a critical reappraisal of the simulation results and a new analysis of the optimal trajectories of a spacecraft equipped with such a propulsion system. The aim of this paper is to review the different thrust models used over the last years for mission analysis purposes, and to illustrate the optimal control law and the corresponding minimum-time trajectories that can be obtained with the new, refined, thrust model. The study highlights new analytical relations for the propulsive thrust as a function of the spacecraft attitude, whereas simple and accurate closed-form equations are also proposed for the study of a classical circle-to-circle coplanar heliocentric orbit transfer.

Key words: Electric solar wind sail, Trajectory optimization, Mission analysis

[1] Associate Professor, a.quarta@ing.unipi.it. **Corresponding author**.

[2] Professor, g.mengali@ing.unipi.it.

1 Introduction

A major constraint in the planning of a space mission is represented by the amount of propellant it requires. The technological advances of the past years have contributed to mitigate such a problem with the development of innovative propulsion means and new mission strategies, which allows a given orbital transfer to be accomplished by minimizing the propellant consumption. In this context, a very promising option is represented by the use of propellantless propulsion systems, which are able of supplying a net thrust to the spacecraft without any reaction mass. Historically, the photonic solar sail [1,2] has been the first propellantless propulsion system to be theoretically proposed and then in-depth analyzed from an engineering viewpoint [3]. Thanks to the new technological availabilities, necessary to build and displace a large gossamer structure, the Japanese probe Interplanetary Kite-craft Accelerated by Radiation Of the Sun (IKAROS) [4,5,6] and the American NanoSail-D2 [7,8,9], have recently demonstrated the effectiveness of a solar sail as a space propulsion system both in a low-Earth orbit and in the interplanetary space. These important experimental proofs of the actual potentialities of a solar sail have much stimulated the research of new mission scenarios [10,11] and new control laws [12], capable of emphasizing the strength of such a propulsion system.

Over the years, other concepts of propellantless propulsion systems have been proposed to the attention of the scientific community, such as the magnetic sail by Zubrin [13,14,15,16] and the Mini-Magnetospheric Plasma Propulsion by Winglee [17,18,19]. More recently, Janhunen [20] has introduced the Electric Solar Wind Sail (E-sail) concept, which consists of thin centrifugally stretched tethers that are maintained charged by an onboard electron gun. The artificial electric field generated by the tethers shields the spacecraft from the solar wind ions that, impacting on it, generate a net thrust in the interplanetary space. For a more in depth discussion about the E-sail general arrangement, the reader is referred to Refs. [21] and [22].

So far, the soundness of the E-sail concept has been checked either by means of laboratory tests, or through accurate plasmadynamic simulations [23,24,25]. A 100 m long E-sail tether is scheduled to fly onboard the Aalto-1 CubeSat, which is planned to be launched into a LEO orbit in late spring 2016 [26,27]. Despite the current availability of theoretical results only, the E-sail concept has received a great interest in the last years, especially for what concerns the preliminary study of its optimal performance in some specific mission scenarios [28,29,30,31,32]. In particular, much efforts have been devoted to the study of a mathematical model able to accurately estimate the E-sail propulsive acceleration, but sufficiently simple to be used within a preliminary mission analysis. In this context, a recent model proposed by Yamaguchi and Yamakawa [33] is able to describe the effects of a spacecraft attitude change on the propulsive thrust modulus and direction. This new model represents a substantial improvement compared to the previous models available so far. In particular, it includes new additional parameters (some of which obtained using experimental data) that increase the degree of accuracy of the estimated thrust.

The aim of this paper is to revise the preliminary mission analysis of an E-sail-based spacecraft and to reassess the study of its optimal control law for a classic interplanetary transfer in the light of this new mathematical thrust model [33]. For the sake of completeness, the paper also briefly describes the different mathematical models used along the years to quantify the E-sail performance . The analysis is able to emphasize some interesting peculiarities of the new model that underpin the development of a fully analytical minimum-time control law for a transfer between heliocentric orbits of given characteristics.

The paper is organized as follows. The next section critically reviews the different mathematical models used so far for mission analysis purposes. Section III illustrates the minimum-time control law for a circle-to-circle heliocentric transfer based on the new thrust model [33]. Section IV reconsiders the same control law and illustrates how an analytical version of it can be obtained. In the last part of the paper the optimal control law is applied to study a

classic mission scenario, constituted by a heliocentric circle-to-circle orbit transfer. Within this context some approximate analytical equations are presented that allow a first order estimate of the mission performance to be obtained without using complex numerical simulations.

2 Review of E-sail thrust models for mission application

Over the last years, the mathematical model of the E-sail propulsive acceleration, used for preliminary mission analysis, underwent important changes. Most of the variations introduced are related to the availability of new and more accurate numerical simulations, mainly of plasmadynamic nature. From a historical viewpoint, the E-sail concept was first proposed by his inventor Janhunen [20] as a sort of evolution of the magnetic sail concept introduced by Zubrin [13,14,15,16]. In Ref. [20] Janhunen estimated the modulus of the propulsive acceleration that can be obtained using a large mesh made of thin conducting wires and kept at a high positive potential with respect to the solar wind plasma. The first orbital simulations involving a spacecraft propelled by an E-sail appeared only three years later in a paper by Janhunen and Sandroos [34]. In particular, the study discussed in appendix C of Ref. [34] assumes a simplified heliocentric scenario in which the E-sail provides a purely radial thrust (in the outward direction) with a modulus that varies with the Sun-spacecraft distance r as $1/r^{7/6}$.

A fundamental performance parameter is the spacecraft characteristic acceleration a_c, that is, the modulus of the propulsive acceleration at a reference distance $r_\oplus \triangleq 1\,\mathrm{au}$ from the Sun. Assuming a circular parking orbit with a radius equal to $r_\oplus$, Ref. [34] discusses a few elementary characteristics of the heliocentric trajectories tracked by an E-sail when its propulsive acceleration vector $\boldsymbol{a}$ is expressed in the form

$$\boldsymbol{a} = a_c \left(\frac{r_\oplus}{r}\right)^{7/6} \hat{\boldsymbol{r}} \tag{1}$$

where $\hat{\boldsymbol{r}} \triangleq \boldsymbol{r}/r$ is the radial unit vector and $\boldsymbol{r}$ is the spacecraft inertial position vector. The

analysis of Ref. [34] is however much simplified, as its main purpose is only to briefly highlight the potentialities of such an innovative propulsion system. The main contribution of Ref. [34] is to give a closed-form expression of the radial and circumferential spacecraft velocity along the propelled trajectory. This result is obtained by noting that, as a consequence of Eq. (1), the spacecraft motion takes place within a conservative force field generated by the gravitational solar attraction and the E-sail thrust. This same characteristic has been subsequently exploited by Mengali and Quarta to calculate the E-sail performance for flyby trajectories toward asteroids [31], or to find an analytical approximation of the E-sail trajectory in the interplanetary space [35].

The first systematic study about mission performance of a spacecraft propelled by an E-sail is found in Ref. [21], where heliocentric transfer trajectories are analyzed within an optimal framework. The mathematical model for the propulsive thrust used in Ref. [21] is a direct evolution of that shown in Eq. (1), as it takes into account the possibility of generating an off-axis propulsive acceleration (that is, a thrust component orthogonal to the radial direction), which is a necessary condition for changing the angular momentum of the spacecraft (in fact, as long as the thrust is along the radial direction, the angular momentum is a constant of motion) and achieving a transfer between two different Keplerian orbits. The off-axis component of the propulsive acceleration can be obtained by changing the angle with which the charged particles of the solar wind collide with the E-sail nominal plane $\mathcal{P}$. The latter is the reference plane containing the sail tethers, which are stretched out by centrifugal force, see Fig. 1.

In Ref. [21] the cone angle $\alpha \in [0, \pi/2]$ is defined as the angle between the radial direction (that is, the direction of $\hat{\boldsymbol{r}}$) and the direction of the propulsive thrust $\boldsymbol{a}$ (that is, the direction of $\hat{\boldsymbol{a}} \triangleq \boldsymbol{a}/\left\|\boldsymbol{a}\right\|$), with

$$\boldsymbol{a} = a_c\,\tau\left(\frac{r_\oplus}{r}\right)^{7/6}\hat{\boldsymbol{a}} \qquad \text{with} \qquad \arccos\left(\hat{\boldsymbol{a}}\cdot\hat{\boldsymbol{r}}\right) \le \alpha_{\max} \tag{2}$$

where $\alpha_{\max}$ is the maximum admissible value of the cone angle, ranging between 20 and 35 deg,

while $\tau \in \{0, 1\}$ is referred to as switching function and is used to model the thruster on/off condition (the latter depending on the electron gun's status). According to Eq. (2), the modulus of the propulsive acceleration $\|\boldsymbol{a}\| = a_c\,\tau\,(r_\oplus/r)^{7/6}$, at a given distance from the Sun, is independent of the cone angle. This characteristic associates the E-sail performance with that of a more conventional solar electric propulsion system.

Using the results from the first plasmadynamic simulations obtained by Janhunen [21], the cone angle α was assumed to be approximately equal to one-half the sail nominal plane's inclination angle $\alpha_n \in [0, \pi]$, referred to as pitch angle. The latter is the angle between the radial direction and that of unit vector $\hat{\boldsymbol{n}}$, normal to the plane $\mathcal{P}$ in the direction opposite to the Sun, see Fig. 2. In other terms, the unit vector $\hat{\boldsymbol{a}}$ lies on the plane containing the unit vectors $\hat{\boldsymbol{r}}$ and $\hat{\boldsymbol{n}}$, except for the particular case of $\alpha_n = 0$ when $\hat{\boldsymbol{a}} \equiv \hat{\boldsymbol{r}}$ (that is, when $\mathcal{P}$ is orthogonal to the radial direction). A maximum cone angle $\alpha_{\max}$ of about $30 - 35\,\mathrm{deg}$ was also assumed in order to prevent the E-sail from the possible occurrence of mechanical instabilities related to a high value of the sail pitch angle (i.e., α_n greater than about $60 - 70\,\mathrm{deg}$).

Subsequent and more refined plasmadynamic simulations [23] allowed Janhunen to estimate a higher thrust level per unit tether length (about five times greater than the former values) and to discover a variation of the propulsive acceleration modulus inversely proportional to the distance from the Sun [36,22]. The new expression for $\boldsymbol{a}$ is similar to that of Eq. (2), but with a different exponent, viz.

$$\boldsymbol{a} = a_c\,\tau\,\left(\frac{r_\oplus}{r}\right)\hat{\boldsymbol{a}} \qquad \text{with} \qquad \arccos\left(\hat{\boldsymbol{a}}\cdot\hat{\boldsymbol{r}}\right) \leq \alpha_{\max} \tag{3}$$

The new relation simplifies the heliocentric motion analysis of the spacecraft in the special case in which the cone angle remains constant during the mission and the characteristic acceleration is sufficiently small compared to the solar gravitational acceleration [37].

Recently, Yamaguchi and Yamakawa [33], with the aid of new numerical simulations, discovered

that the variation of α with α_n is more complex than a simple linear law. Using a best-fit interpolation of numerical data, the following polynomial relation between α and α_n was obtained [33]

$$\alpha = b_6\,\alpha_n^6 + b_5\,\alpha_n^5 + b_4\,\alpha_n^4 + b_3\,\alpha_n^3 + b_2\,\alpha_n^2 + b_1\,\alpha_n + b_0 \tag{4}$$

where the coefficients b_i, with $i = 1, 2, \ldots, 6$ are summarized in Tab. 1 (the same table also fixes a few typos in the original paper [33]).

The analysis of Ref. [33] points out that, for a given Sun-spacecraft distance r, the propulsive acceleration modulus $\|\boldsymbol{a}\|$ is strongly dependent on the E-sail attitude through the pitch angle α_n. This is clearly shown by the dimensionless acceleration γ, defined as the ratio between the modulus of the propulsive acceleration at an angle α_n to the maximum propulsive acceleration at a distance r from the Sun

$$\gamma \triangleq \frac{\|\boldsymbol{a}\|}{a_c\ (r_\oplus/r)} \tag{5}$$

According to the procedure described in Ref. [33], a best-fit interpolation of numerical data gives

$$\gamma = c_6\,\alpha_n^6 + c_5\,\alpha_n^5 + c_4\,\alpha_n^4 + c_3\,\alpha_n^3 + c_2\,\alpha_n^2 + c_1\,\alpha_n + c_0 \tag{6}$$

where the coefficients c_i are summarized in Tab. 1.

Figure 3 shows the variations of α and γ (described by Eqs. (4)-(6)) with the pitch angle α_n. The linear variation of the cone angle with the pitch angle in the form $\alpha \simeq \alpha_n/2$ is in good agreement with the numerical simulations of Ref. [33] until $\alpha_n \leq 20\,\text{deg}$. When $\alpha_n > 20\,\text{deg}$, the function $\alpha = \alpha(\alpha_n)$ has a marked nonlinear behavior. It reaches a maximum value, slightly less than 20 deg, when $\alpha_n \simeq 55\,\text{deg}$, then it decreases quickly and goes to zero at $\alpha_n = 90\,\text{deg}$. The dimensionless propulsive acceleration, instead, reaches its maximum ($\gamma = 1$) at $\alpha_n = 0$, when the Sun-spacecraft line is normal to the E-sail nominal plane $\mathcal{P}$. Note that γ decreases monotonically with α_n until it reaches a minimum value of about 0.5 at $\alpha_n = 90\,\text{deg}$. Figure 3(b) also shows that the propulsive acceleration is about 70% of its maximum value (that is, $\gamma \simeq 0.7$)

when the cone angle takes its maximum value. However, the case in which $\alpha_n > 60 - 70\,\text{deg}$ is likely to be unreachable due to the presence of possible mechanical instabilities [21]. For this reason the two curves of Fig. 3 should be used within a reduced range of variation of α_n, that is, in a simplified way, in the range $\alpha_n \in [0, 60]\,\text{deg}$.

Bearing in mind that the propulsive acceleration vector lies on the plane containing $\hat{\boldsymbol{r}}$ and $\hat{\boldsymbol{n}}$, that $\hat{\boldsymbol{a}} \equiv \hat{\boldsymbol{r}}$ when $\alpha_n = 0$, and that its modulus is inversely proportional to the Sun-spacecraft distance, the following vectorial relation is obtained

$$\boldsymbol{a} = \begin{cases} a_c\,\tau\,\left(\dfrac{r_\oplus}{r}\right)\,\gamma\,\left[\dfrac{\sin\left(\alpha_n - \alpha\right)}{\sin\alpha_n}\,\hat{\boldsymbol{r}} + \dfrac{\sin\alpha}{\sin\alpha_n}\,\hat{\boldsymbol{n}}\right] & \text{if} \quad \alpha_n \in (0,\,\pi/2] \\ \\ a_c\,\tau\,\left(\dfrac{r_\oplus}{r}\right)\,\hat{\boldsymbol{r}} & \text{if} \quad \alpha_n = 0 \end{cases} \tag{7}$$

For a given position vector $\boldsymbol{r}$, Eq. (7) states that the propulsive acceleration vector is a function of the orientation of the normal unit vector $\hat{\boldsymbol{n}}$ only (this amounts to state that the direction of $\boldsymbol{a}$ is uniquely defined by means of two scalar independent variables). In fact, $\cos\alpha_n = \hat{\boldsymbol{n}} \cdot \hat{\boldsymbol{r}}$, and recall that γ and α are both functions of α_n, see Eqs. (4) and (6). Note that the old model (3) coincides with the refined model of Ref. [33] when $\alpha_n = 0$, that is, in case of purely radial thrust. This implies that all of the results obtained in previous studies involving the E-sail dynamics under a radial thrust [31,35] remain valid under the new thrust model.

To summarize, the different E-sail thrust models available for preliminary mission analysis are summarized by Eqs. (2), (3) and (7). The first two models, Eqs. (2) and (3), have been used to analyze different mission scenarios (some of which using an optimal approach) and the results obtained are reported in Refs. [21,37,38,39,40]. As far as the refined model by Yamaguchi and Yamakawa [33] is concerned, so far it has been used only in the mission analyses discussed in Refs. [32,41], which are not performed within an optimal framework. For this reason the next section analyzes the classical minimum time transfer problem between two heliocentric circular and coplanar orbits using the thrust model described by Eq. (7). This allows the two thrust

models (3) and (7) to be compared using the same mission scenario. New insights involving the new thrust model will also be proposed, thus extending the results discussed in Ref. [33].

3 Circle-to-circle optimal transfer analysis

Consider a two-dimensional heliocentric scenario, in which an E-sail-based spacecraft with a characteristic acceleration a_c is placed along a circular parking orbit of radius r_0. The spacecraft must be transferred to a circular final orbit, coplanar to the first one, with radius r_1. The problem is conveniently described by introducing a polar heliocentric frame of reference $\mathcal{T}_\odot(O; r, \theta)$, whose origin O coincides with the Sun's barycenter, $\hat{\boldsymbol{i}}_\theta$ is the transverse unit vector, and θ is the polar angle measured counterclockwise from the SunŰspacecraft direction at the initial time instant $t_0 \triangleq 0$, see Fig. 4. By assumption, the unit vector $\hat{\boldsymbol{n}}$ lies in the plane of the two circular orbits. For this reason the definition of the pitch angle (and so the definition of the cone angle) is now slightly revised to account for the two possible cases $\hat{\boldsymbol{n}} \cdot \hat{\boldsymbol{i}}_\theta > 0$ or $\hat{\boldsymbol{n}} \cdot \hat{\boldsymbol{i}}_\theta < 0$. To that end, without loss of generality, the pitch angle is assumed to vary in the range $\alpha_n \in [-\pi/2,\, \pi/2]$, and the components of $\hat{\boldsymbol{n}}$ in the frame $\mathcal{T}_\odot$ are therefore

$$[\hat{\boldsymbol{n}}]_{\mathcal{T}_\odot} = [\cos\alpha_n,\ \sin\alpha_n]^{\mathrm{T}} \tag{8}$$

A positive (negative) value of the pitch angle corresponds to a situation in which the transverse component of the propulsive thrust tends to increase (decrease) the modulus of the angular momentum of the osculating orbit.

The introduction of a negative value of the pitch angle requires a formal variation of the two Eqs. (4) and (6) that define the thrust characteristics as a function of the control variables. More precisely, taking into account that γ is always positive, see Eq. (5), and that the sign of

α follows that of α_n, Eqs. (4) and (6) are now rewritten as

$$\alpha = \text{sign}\,(\alpha_n)\,\left(b_6\,\alpha_n^6 + b_5\,|\alpha_n|^5 + b_4\,\alpha_n^4 + b_3\,|\alpha_n|^3 + b_2\,\alpha_n^2 + b_1\,|\alpha_n| + b_0\right) \tag{9}$$

$$\gamma = c_6\,\alpha_n^6 + c_5\,|\alpha_n|^5 + c_4\,\alpha_n^4 + c_3\,|\alpha_n|^3 + c_2\,\alpha_n^2 + c_1\,|\alpha_n| + c_0 \tag{10}$$

where sign $(\square)$ is the signum function, and the coefficients b_i and c_i are those of Tab. 1. The new variation of γ and α with α_n is shown in Fig. 5. Note that $\alpha(\alpha_n)$ is an odd function, whereas $\gamma(\alpha_n)$ is an even function of the pitch angle.

The spacecraft equations of motion can be written as

$$\dot{r} = u \tag{11}$$

$$\dot{\theta} = v/r \tag{12}$$

$$\dot{u} = \frac{v^2}{r} - \frac{\mu_\odot}{r^2} + a_r \tag{13}$$

$$\dot{v} = -\frac{u\,v}{r} + a_\theta \tag{14}$$

where $\mu_\odot$ is the Sun's gravitational parameter, u (or v) is the radial (or transverse) component of the spacecraft velocity, whereas a_r and a_θ are the two components of the spacecraft propulsive acceleration in the polar reference frame. From Eqs. (7) and (8) it is found that

$$a_r = a_c\,\tau\,\left(\frac{r_\oplus}{r}\right)\,\gamma\,\cos\alpha \tag{15}$$

$$a_\theta = a_c\,\tau\,\left(\frac{r_\oplus}{r}\right)\,\gamma\,\sin\alpha \tag{16}$$

where γ and α are given by Eqs. (9)-(10) as a function of the pitch angle. To summarize, the heliocentric two-dimensional dynamics of the spacecraft is described by the equations of motion (11)-(14), where τ and α_n are the two control variables. The switching function regulates the activation status of the propulsion system (and the corresponding presence of possible coasting arcs along the trajectory), while the pitch angle adjusts the direction (and so the modulus)

of the propulsive acceleration. The control law for τ and α_n can be obtained by solving an optimal control problem, as is described in the next section.

3.1 Trajectory optimization

The E-sail mission is now analyzed within an optimal framework by looking for the minimum flight time $\Delta t^\star \triangleq \min(t_1 - t_0) \equiv \min(t_1)$, where t_1 is the time at the end of the transfer. The problem amounts to maximizing the performance index $J \triangleq -t_1$. The optimal control law will be found using an indirect approach, thus allowing for a direct comparison between the results obtained with the thrust model of Eq. (7) and those previously discussed in [42,43] using the model of Eq. (3).

Paralleling the procedure described in Ref. [42], the Hamiltonian function $\mathcal{H}$ of this problem is

$$\mathcal{H} \triangleq \lambda_r\, u + \lambda_\theta\, \frac{v}{r} + \lambda_u \left(\frac{v^2}{r} - \frac{\mu_\odot}{r^2} \right) - \lambda_v\, \frac{u\, v}{r} + \mathcal{H}' \tag{17}$$

where λ_r, λ_θ, λ_u and λ_v are the adjoint variables associated with the state variables r, θ, u, and v, respectively, and $\mathcal{H}'$ coincides with that portion of the Hamiltonian that explicitly depends on the controls $\{\tau, \alpha_n\}$, or

$$\mathcal{H}' \triangleq a_c\, \tau\, \gamma\, \left(\frac{r_\oplus}{r} \right)\, (\lambda_u\, \cos\alpha + \lambda_v\, \sin\alpha) \tag{18}$$

The time derivatives of the adjoint variables are given by the Euler-Lagrange equations

$$\dot{\lambda}_r \triangleq -\frac{\partial \mathcal{H}}{\partial r} = \frac{\lambda_\theta\, v}{r^2} + \lambda_u \left(\frac{v^2}{r^2} - \frac{2\,\mu_\odot}{r^3} \right) - \lambda_v\, \frac{u\, v}{r^2} + \frac{\mathcal{H}'}{r} \tag{19}$$

$$\dot{\lambda}_\theta \triangleq -\frac{\partial \mathcal{H}}{\partial \theta} = 0 \tag{20}$$

$$\dot{\lambda}_u \triangleq -\frac{\partial \mathcal{H}}{\partial u} = -\lambda_r + \lambda_v\, \frac{v}{r} \tag{21}$$

$$\dot{\lambda}_v \triangleq -\frac{\partial \mathcal{H}}{\partial v} = -\frac{\lambda_\theta}{r} - 2\, \frac{\lambda_u\, v}{r} + \frac{\lambda_v\, u}{r} \tag{22}$$

Note that, according to Eq. (20), the adjoint variable λ_θ is a constant of motion.

From Pontryagin's maximum principle, the optimal control law must maximize, at any time, the function $\mathcal{H}'$ given by Eq. (18). To that end, it is useful to introduce an auxiliary angle $\delta \in [-\pi,\, \pi]$, depending on the pair $\{\lambda_u,\, \lambda_v\}$, defined as [42]

$$\cos\delta \triangleq \frac{\lambda_u}{\sqrt{\lambda_u^2+\lambda_v^2}} \quad , \quad \sin\delta \triangleq \frac{\lambda_v}{\sqrt{\lambda_u^2+\lambda_v^2}} \tag{23}$$

Note that δ can be thought of as a sort of cone angle of Lawden's primer vector [44], whose components, in the reference frame $\mathcal{T}_\odot$, are just λ_u and λ_v. Equation (18) can therefore be rewritten as

$$\mathcal{H}' = a_c \left(\frac{r_\oplus}{r}\right) \sqrt{\lambda_u^2+\lambda_v^2}\, \tau\, \mathcal{H}'_{\alpha_n} \quad \text{with} \quad \mathcal{H}'_{\alpha_n} \triangleq \gamma\,(\cos\delta\, \cos\alpha + \sin\delta\, \sin\alpha) \tag{24}$$

where $\mathcal{H}'_{\alpha_n}$ is the portion of $\mathcal{H}'$ that depends on the pitch angle only, see Eqs. (9)-(10). For a given value of δ, the optimal pitch angle $\alpha_n^\star$ solves the problem

$$\alpha_n^\star = \max_{\alpha_n} \left(\mathcal{H}'_{\alpha_n}\right) \tag{25}$$

The function $\mathcal{H}'_{\alpha_n}$ is maximized with a numerical algorithm based on a golden section search and parabolic interpolation [45]. The results obtained from Eq. (25) are reported in Fig. 6. In particular, Fig. 6(a) shows $\alpha_n^\star$ as a function of δ, while the corresponding maximum value of $\mathcal{H}'_{\alpha_n}$ is illustrated in Fig. 6(b). The relation between $\alpha_n^\star$ and δ turns out to be linear and in the form $\alpha_n^\star = \delta/2$. The analytical proof of this result is postponed and will be given in the next section. Figure 6(b) shows that $\max(\mathcal{H}'_{\alpha_n}) < 0$ when $|\delta| > \widetilde{\delta}$, where $\widetilde{\delta} \simeq 110\,\text{deg}$ is a sort of critical primer vector's cone angle. This is an important result, which is closely related to the optimal value of the switching function τ. In fact, from Eq. (18) the reduced Hamiltonian $\mathcal{H}'$ is a linear function of τ, and its sign coincides with the sign of $\mathcal{H}'_{\alpha_n}$. Accordingly, the optimal value of τ is given by

$$\tau^\star = \frac{\text{sign}\left(\widetilde{\delta} - |\delta|\right) + 1}{2} \tag{26}$$

This last equation implies that the maximum value of $\mathcal{H}'$, and so the maximum of $\mathcal{H}$, is obtained by switching the propulsion system on ($\tau^\star = 1$) when $|\delta| \leq \widetilde{\delta}$, or off ($\tau^\star = 0$) when $|\delta| > \widetilde{\delta}$. The optimal control law involving the two control variables α_n and τ, is drawn in Fig. 7.

The same control problem can also be addressed by looking for the optimal values of cone angle ($\alpha = \alpha^\star$) and dimensionless propulsive acceleration $\gamma = \gamma^\star$ as a function of δ. The results are summarized in Fig. 8. The two curves are obtained using the information taken from Fig. 7 and substituting Eq. (25) into Eqs. (9)-(10).

Notably, the optimal control law exploits the whole admissible range of variation of the cone angle, cfr. Fig. 5(a), where the extreme values of α, about $\pm 20\,\mathrm{deg}$, are reached when the primer vector's cone angle is close to $\widetilde{\delta}$. Also note that the optimal control law with the new thrust model is substantially different from that discussed in Ref. [42] using the thrust model given by Eq. (2).

The optimal values of the trust components, that is $a_r^\star$ and $a_\theta^\star$, are calculated by substituting the expressions of $\alpha^\star$ and $\tau^\star$ into Eqs. (15)-(16). Figure 9 illustrates how these optimal dimensionless components vary with δ. The maximum value of the circumferential component turns out to be within the admissible range of variation of δ. This is an important point, since the presence of a circumferential thrust component allows the angular momentum of the osculating orbit to be changed. Also note that the maximum value of $|a_\theta^\star|$ takes place when $\delta = \pm 90\,\mathrm{deg}$. A mathematical explanation for this result is possible, and will be given in the next section.

Having found the optimal control law, which is summarized in Fig. 7, where the angle δ is given by Eqs. (23), the minimum time transfer problem can be solved by numerically integrating the four equations of motion (11)–(14) and the four Euler-Lagrange equations (19)–(22). The differential problem is completed by eight boundary conditions at the initial time t_0 and at the final time t_1. Exploiting the polar symmetry of the problem, the four boundary conditions at

t_0 are

$$r(t_0) = r_0 \quad , \quad \theta(t_0) = 0 \quad , \quad u(t_0) = 0 \quad , \quad v(t_0) = \sqrt{\frac{\mu_\odot}{r_0}} \tag{27}$$

Assuming that the angular position of the spacecraft along the final orbit is left free, the four boundary conditions at t_1 become

$$r(t_1) = r_1 \quad , \quad \lambda_\theta(t_1) = 0 \quad , \quad u(t_1) = 0 \quad , \quad v(t_1) = \sqrt{\frac{\mu_\odot}{r_1}} \tag{28}$$

The optimal mission time is obtained by enforcing the transversality condition [46] $\mathcal{H}(t_1) = 1$.

4 Analytical form of the optimal control law

In view of the peculiarity of some results obtained in the last section, especially the linear relation of the optimal pitch angle with δ, the suspicion exists that an analytical form of the optimal control law may be recovered. It will now be shown that this is indeed possible. To that end it is first useful to draw the circumferential propulsive acceleration a_θ as a function of the radial component a_r when the propulsion system is on ($\tau = 1$). Substituting Eqs. (9)-(10) into Eqs. (15)-(16), the two components of propulsive acceleration are shown in dimensionless form in Fig. 10 (the normalization factor $a_c\,(r_\oplus/r)$ is the maximum propulsive acceleration at a generic distance from the Sun). The dotted lines of Fig. 10 correspond to the locus of points having the same value of α. The figure clearly shows that the relation $a_r = a_r(a_\theta)$ can be accurately approximated (in a dimensionless form) through a circle with center $C = (0,\, d)$ and radius R, where

$$d = \frac{\gamma(\alpha_n = 0) + \gamma(\alpha_n = \pi/2)}{2} \simeq 0.7477 \tag{29}$$

$$R = \frac{\gamma(\alpha_n = 0) - \gamma(\alpha_n = \pi/2)}{2} \simeq 0.2523 \tag{30}$$

and γ is taken from Eq. (10). The two propulsive acceleration components, including the presence of the switching function τ, can be more conveniently rewritten in a parametric form

with the aid of a new angular coordinate $\nu \in [0,\, 2\,\pi]$, see Fig. 10. The result is

$$a_r = a_c \left(\frac{r_\oplus}{r}\right) \tau \, (d + R \, \cos\nu) \qquad , \qquad a_\theta = a_c \left(\frac{r_\oplus}{r}\right) \tau \, R \, \sin\nu \tag{31}$$

from which it is apparent that ν plays the role of an auxiliary control variable in the same way as the pitch angle α_n does in the original formulation of the refined thrust model.

By direct comparison between Eqs. (31) and Eqs. (15)-(16) it is found that

$$\gamma \, \cos\alpha = d + R \, \cos\nu \qquad , \qquad \gamma \, \sin\alpha = R \, \sin\nu \tag{32}$$

Squaring and summing the last two equations, the dimensionless propulsive acceleration γ is written as a function of the triplet $\{d, R, \nu\}$ as

$$\gamma = \sqrt{d^2 + R^2 + 2 \, R \, d \, \cos\nu} \tag{33}$$

while the cone angle α becomes

$$\alpha = \arctan\left(\frac{R \, \sin\nu}{d + R \, \cos\nu}\right) \tag{34}$$

It can be verified that Eqs. (33) and (34) are equivalent to the original Eqs. (10) and (9), provided that

$$\nu = 2 \, \alpha_n \tag{35}$$

The latter claim is confirmed by Fig. 11, which compares the two functions $\gamma = \gamma(\alpha_n)$ and $\alpha = \alpha(\alpha_n)$ obtained using the results from Ref. [33] and the analytical approximations of Eqs. (33)–(35). The soundness of Eqs. (33)–(35) can also be confirmed through the optimal control law obtained using ν as the control variable in place of the pitch angle. In fact, when Eqs. (32) are substituted into Eq. (24), the resulting expression for $\mathcal{H}'$ is

$$\mathcal{H}' = a_c \left(\frac{r_\oplus}{r}\right) \sqrt{\lambda_u^2 + \lambda_v^2} \, \tau \, \mathcal{H}'_\nu \quad \text{with} \quad \mathcal{H}'_\nu \triangleq \cos\delta \, (d + R \, \cos\nu) + R \, \sin\delta \, \sin\nu \tag{36}$$

The optimal value $\nu^\star$ of the auxiliary control variable is obtained by maximizing the function

$\mathcal{H}'_\nu$. From the necessary condition $\partial\mathcal{H}'_\nu/\partial\nu = 0$ it is found that

$$\nu^\star = \delta \tag{37}$$

Therefore, in an optimal transfer, the angular variable ν coincides with the primer vector's cone angle δ. Substituting Eq. (35) into (37), the optimal pitch angle is $\alpha_n^\star = \delta/2$, which is in accordance with the previous results of Fig. 6(a). Substituting Eq. (37) into (34), the analytical form of the optimal control law for the cone angle is

$$\alpha^\star = \arctan\left(\frac{R\,\sin\delta}{d + R\,\cos\delta}\right) \tag{38}$$

which overlaps exactly with that drawn in Fig. 8 when $\tau = 1$. Likewise, using Eq. (33), the optimal expression for the dimensionless propulsive acceleration is

$$\gamma^\star = \sqrt{d^2 + R^2 + 2\,R\,d\,\cos\delta} \tag{39}$$

The maximum value of $\mathcal{H}'_\nu$ is obtained by substituting Eq. (37) into the second of Eqs. (36), that is

$$\max\left(\mathcal{H}'_\nu\right) = d\,\cos\delta + R \tag{40}$$

Recall that $\mathcal{H}'$ depends linearly on τ, see Eq. (36), and note that the sign of $\mathcal{H}'$ coincides with that of $\mathcal{H}'_\nu$. From Eq. (40), the optimal switching function is found as

$$\tau^\star = \begin{cases} 0 & \text{when} \quad \delta > \arccos\left(-R/d\right) \\ \\ 1 & \text{when} \quad \delta \leq \arccos\left(-R/d\right) \end{cases} \tag{41}$$

where $\arccos\left(-R/d\right) \simeq 109.7\,\text{deg}$, using the values of d and R from Eqs. (29)-(30). The control law (41) is therefore equivalent to the previous Eq. (26) since $\widetilde{\delta} \simeq \arccos\left(-R/d\right)$. Notably, Eq. (41) has a nice geometrical interpretation, illustrated in Fig. 12. In particular, the arc of circle corresponding to $\tau = 0$ is bounded by two half-lines from the origin and tangent to the circle that describes the variation of the two acceleration components. From the geometrical

interpretation of Fig. 12, the maximum cone angle is found as

$$\alpha_{\max} = \arccos\left(-R/d\right) - \frac{\pi}{2} \tag{42}$$

that is, about 20 deg, which is in agreement with the results of Fig. 8.

In conclusion, the optimal values of the propulsive acceleration components have the following analytical expressions

$$a_r^\star = a_c \left(\frac{r_\oplus}{r}\right) \frac{\text{sign}\left(\arccos\left(-R/d\right) - |\delta|\right) + 1}{2} \left(d + R\,\cos\delta\right) \tag{43}$$

$$a_\theta^\star = a_c \left(\frac{r_\oplus}{r}\right) \frac{\text{sign}\left(\arccos\left(-R/d\right) - |\delta|\right) + 1}{2} R\,\sin\delta \tag{44}$$

which coincide with the results illustrated in Fig. 9. In particular, the maximum value of the circumferential acceleration component is reached when the modulus of the primer vector's cone angle equals 90 deg.

To summarize, the two-point boundary value problem to be solved is constituted by the eight differential equations (11)–(14) and (19)–(22), along with the eight initial conditions (27)–(28) and the transversality equation $\mathcal{H}(t_1) = 1$ (the latter is necessary to calculate the flight time). The components of the propulsive acceleration a_r and a_θ are obtained from Eqs. (43)–(44) and δ is given by Eqs. (23). A simplification to the problem is obtained by noting that when Eq. (20) is combined with the second of (28), the adjoint variable λ_θ is zero for all $t \in [t_0,\, t_1]$.

5 Numerical simulations

The optimal control law discussed in the last section has been used to simulate minimum-time circle-to-circle transfers of an E-sail-based spacecraft starting from a circular heliocentric orbit of radius $r_0 \triangleq 1$ au. This scenario is representative, for example, of an E-sail deployment on a parabolic Earth escape trajectory with zero hyperbolic excess energy with respect to the

planet.

In all of the simulations, the E-sail characteristic acceleration is assumed to be $a_c = 1\,\mathrm{mm/s^2}$. Even though such a value is representative of a an E-sail with medium-high performance, it is usually referred to as "canonical" value, in analogy with a similar definition adopted for photonic solar sails [2]. It also represents an useful reference parameter for performance comparisons between different thrust models. The characteristic acceleration, of course, depends on the spacecraft mass and, therefore, on the payload mass. For example, using the mass breakdown model discussed in Ref. [47], a value of $a_c = 1\,\mathrm{mm/s^2}$ could (theoretically) be obtained with a spacecraft having a total mass of about 400 kg with a payload mass of 100 kg.

Figure 13 summarizes a parametric study in which the minimum flight time $\Delta t^\star$ is shown for different values of the final orbital radius in the range $r_1 \in [0.3,\, 1.6]\,\mathrm{au}$. The figure also shows a comparison with the minimum flight time that can be obtained with a classical thrust model, described by Eq. (3), and a maximum cone angle of $\alpha_{\max} = 30\,\mathrm{deg}$. As expected, the performance (in terms of transfer times) with the new thrust model are much worse than those attainable with a classical model. This is mainly due to the different values of the maximum value of the cone angle between the two models (about 20 deg in the new model, compared to about 30 deg in the previous one). The performance differences tend to markedly increase as the final radius becomes smaller, due to a higher complexity of the resulting spacecraft trajectory, with an increasing number of revolutions around the Sun and a number of coasting arcs along the trajectory. This problem is highlighted in Fig. 14, which shows the transfer trajectories for different values of r_1.

The flight time varies considerably also as a function of the spacecraft characteristic acceleration. In this context, the dependence of $\Delta t^\star$ on a_c has been studied in the special case of $r_0 = 1\,\mathrm{au}$ and $r_1 = 1.524\,\mathrm{au}$, which is representative of an Earth-Mars transfer when the eccentricity of the planetary orbits and their relative inclination are both neglected. The optimal

transfer problem is solved under the assumption of free planetary ephemerides (that is, the final angular position of the spacecraft along the Mars' orbit is left free), which amounts to finding the minimum flight time between the two heliocentric orbits. The results are reported in Fig. 15 as a function of $a_c \in [0.1,\, 1]\,\mathrm{mm/s^2}$ for the two different thrust models. Taking the performance corresponding to a classical thrust model as a reference value, the flight time obtained with the new model (solid line) is increased of about 30% when $a_c = 1\,\mathrm{mm/s^2}$, while the difference between the two transfer times is even 1500 days (with an increase of 100%) when $a_c = 0.1\,\mathrm{mm/s^2}$. The increased complexity of the spacecraft trajectory when the value of a_c is decreased, is shown in Fig. 16.

In particular, when the value of a_c is sufficiently small, the transfer trajectory resembles a spiral without coasting arcs. In fact, when the propulsive acceleration is much smaller than the solar gravitational acceleration, the transfer between the initial and the final orbit takes place as if the spacecraft were continuously moved along a series of circular orbits with an increasing radius. Such a characteristic is clearly illustrated in Fig. 17, which shows the simulation results corresponding to $a_c = 0.1\,\mathrm{mm/s^2}$. Note that the time variations of the radial (u) and circumferential (v) velocity components are normalized with the local circular velocity ($\sqrt{\mu_\odot / r}$). The time scale is also normalized with the minimum flight time, equal to $\Delta t^\star \simeq 3281$ days. Figure 17 also shows the time variation of the cone angle ($\alpha^\star$) and of the angular momentum of the osculating orbit

$$h \triangleq r\, v \tag{45}$$

In particular, the time variation of h has been normalized using either the angular momentum of the initial orbit ($\sqrt{\mu_\odot\, r_0}$), or using the angular momentum of the local circular orbit ($\sqrt{\mu_\odot\, r}$). Figure 17 shows that the optimal cone angle $\alpha^\star$ has small oscillations around a nearly constant mean value $\overline{\alpha}$. The latter, of about 18 deg, is close to the maximum admissible value ($\alpha_{\max} \cong 20$ deg). The reason is that when a_c is small, the orbital radius variation is obtained, at each distance r from the Sun, by exploiting the maximum circumferential component of the

propulsive thrust a_θ. Bearing in mind Eq. (35) and recalling Fig. 10, the maximum value of a_θ is obtained when $\alpha_n = \pi/4$. The latter corresponds to a cone angle $\alpha \simeq 18.6\,\text{deg}$, see Eq. (4), which is close to the mean value obtained from Fig. 17.

The fact that the cone angle is about constant during the whole transfer is confirmed by the linearity of the function $h = h(t)$, as is shown in Fig. 17. The reason is that if the cone angle is about constant (and equal to $\overline{\alpha}$), so is the pitch angle (which is about equal to its mean value $\overline{\alpha}_n$). Under the assumption that the propulsion system is on ($\tau = 1$) along the whole flight, and using the Eq. (16) for a_θ, the equation of motion (14) can be written as

$$\dot{h} = r\, a_\theta \equiv a_c\, r_\oplus\, \gamma\, \sin\alpha \tag{46}$$

As long as the pitch angle is constant, i.e. $\alpha_n = \overline{\alpha}_n$, the dimensionless propulsive acceleration is about constant and equal to its mean value $\overline{\gamma}$. The right hand side of Eq. (46) is therefore a constant of motion, and the approximate law of variation of the angular momentum becomes

$$h \simeq \sqrt{\mu_\odot\, r_0} + (a_c\, r_\oplus\, \overline{\gamma}\, \sin\overline{\alpha})\; t \tag{47}$$

where $\sqrt{\mu_\odot\, r_0}$ is the value of h at the initial time, that is, along a circular orbit of radius r_0. Note that Eq. (47) is consistent with the results discussed in Ref. [37], where the dynamics of an E-sail was investigated under the assumption of constant value of pitch angle.

Figure 17 also shows that the instantaneous value of h oscillates around $\sqrt{\mu_\odot\, r}$, which corresponds to the angular momentum of the local circular orbit. Substituting the equation

$$h \simeq \sqrt{\mu_\odot\, r} \tag{48}$$

into Eq. (47), the minimum flight time can be approximated as

$$\Delta t^\star \simeq \frac{\sqrt{\mu_\odot\, r_1} - \sqrt{\mu_\odot\, r_0}}{a_c\, r_\oplus\, \overline{\gamma}\, \sin\overline{\alpha}} \tag{49}$$

where, assuming $\alpha_n = \pi/4$, one has $\overline{\gamma} \simeq 0.7891$ and $\overline{\alpha} \simeq 18.6\,\text{deg}$. For example if $a_c =$

$0.1\,\mathrm{mm/s^2}$, $r_0 = 1\,\mathrm{au}$, $r_1 = 1.524\,\mathrm{au}$, and from Eq. (49) the flight time is $\Delta t^\star \simeq 3204\,\mathrm{days}$, which differs of 2.3% only from the actual value of 75 days.

The soundness of approximation (49) depends on the characteristic acceleration value, which must be sufficiently small as confirmed by Fig. 18. Note that the results for an Earth-Mars transfer are in good agreement with those obtained with the simplified formula (49) if $a_c \leq 0.15\,\mathrm{mm/s^2}$. This is an important point, since the simulations of the optimal trajectory may be affected by convergence problems for small values of the characteristic acceleration due to the high sensitivities of the adjoint variables to their (unknown) initial conditions. As a final remark, Eq. (49) is to be applied for an orbit raising case, or $r_1 > r_0$. It can however be verified that when $r_1 < r_0$, the same Eq. (49) is still valid by simply changing the sign of $\overline{\alpha}$, that is, using $\overline{\alpha} \simeq -18.6\,\mathrm{deg}$.

6 Conclusions

A thorough analysis of the new thrust model allowed us to obtain new information about the potentialities of an Electric Solar Wind Sail for mission applications. The study of minimum-time heliocentric missions for a classic circle-to-circle coplanar transfer has clearly shown that the Electric Solar Wind Sail performance attainable with the new model are definitely lower than those calculated in the past. Nevertheless, this does not imply that the results obtained with the previous model have become useless. In fact, the new model and the old one are substantially coincident (in terms of thrust vector) for small pitch angles. This kind of thrust strategy, which amounts to a nearly radial propulsive acceleration outward from the Sun, is particularly simple to obtain due to the natural tendency of the Electric Solar Wind Sail to orient its nominal plane orthogonal to the Sun-spacecraft direction. In other terms, the Electric Solar Wind Sail performance calculated with the old thrust model are essentially equivalent to that attainable with the new model until the cone angle remains sufficiently small.

The new thrust model is able to take into account (within some limits) the effects of a spacecraft attitude variation in the preliminary mission analysis. It is known, however, that not all of the physical phenomena have been modelled. In particular, the thrust model neglects the variability of the solar wind characteristics and implicitly assumes the existence of a closed loop control system for continuously adjusting the tether voltage and modulating the thrust intensity. Further improvements are therefore possible, even though the model complexity could probably reach a so high degree of complexity that it could be hardly applicable to a preliminary mission analysis. Nevertheless, further refinements of the mathematical model are necessary for obtaining new confirmations about the actual Electric Solar Wind Sail capability of balancing the local fluctuations of the solar wind.

References

[1] L. Friedman, Starsailing: Solar Sails and Interstellar Travel, 1st Edition, Science Editions, Wiley, 1988, Ch. 1, ISBN:978-0471625933.

[2] C. R. McInnes, Solar Sailing: Technology, Dynamics and MissionApplications, Space Science and Technology, Springer-Verlag, Berlin, 1999, pp. 1–14.

[3] J. Wright, Space Sailing, 1st Edition, Routledge, 1992, Ch. 4, pp. 93–121, ISBN: 978-2881248429.

[4] Y. Tsuda, O. Mori, R. Funase, S. Hirotaka, T. Yamamoto, T. Saiki, T. Endo, K. Yonekura, H. Hoshino, J. Kawaguchi, Achievement of IKAROS - japanese deep space solar sail demonstration mission, in: G. Genta (Ed.), Missions to the Outer Solar System and Beyond, Seventh IAA Symposium on Realistic Near-Term Advanced Scientific Space Missions, Aosta, Italy, 2011.

[5] Y. Tsuda, O. Mori, R. Funase, H. Sawada, T. Yamamoto, T. Saiki, T. Endo, J. Kawaguchi, Flight status of IKAROS deep space solar sail demonstrator, Acta Astronautica 69 (9-10) (2011) 833–840, doi: 10.1016/j.actaastro.2011.06.005.

[6] O. Mori, Y. Tsuda, Y. Shirasawa, T. Saiki, Y. Mimasu, J. Kawaguchi, Attitude control of IKAROS solar sail spacecraft and its flight results, in: 61st International Astronautical Congress, Prague, Czech Republic, 2010, paper IAC-10.C1.4.3.

[7] L. Johnson, M. Whorton, A. Heaton, R. Pinson, G. Laue, C. Adams, NanoSail-D: A solar sail demonstration mission, Acta Astronautica 68 (5-6) (2011) 571–575, doi: 10.1016/j.actaastro.2010.02.008.

[8] L. Johnson, R. Young, N. Barnes, L. Friedman, V. Lappas, C. R. McInnes, Solar sails: Technology and demonstration status, International Journal of Aeronautical and Space Sciences 13 (4) (2012) 421–427, doi: 10.5139/IJASS.2012.13.4.421.

[9] L. Johnson, R. Young, E. Montgomery, D. Alhorn, Status of solar sail technology within NASA, Advances in Space Research 48 (11) (2011) 1687–1694, doi: 10.1016/j.asr.2010.12.011.

[10] R. J. McKay, M. Macdonald, J. D. Biggs, C. R. McInnes, Survey of highly-non-keplerian orbits with low-thrust propulsion, Journal of Guidance, Control, and Dynamics 34 (3) (2011) 645–666, doi: 10.2514/1.52133.

[11] G. Aliasi, G. Mengali, A. A. Quarta, Artificial lagrange points for solar sail with electrochromic material panels, Journal of Guidance, Control, and Dynamics 36 (5) (2013) 1544–1550, doi: 10.2514/1.58167.

[12] A. A. Quarta, G. Mengali, Approximate solutions to circle-to-circle solar sail orbit transfer, Journal of Guidance, Control, and Dynamics 36 (6) (2013) 1866–1890, doi: 10.2514/1.60307.

[13] D. G. Andrews, R. M. Zubrin, Use of magnetic sails for mars exploration missions, in: AIAA/ASME/SAE/ASEE 25th Joint Propulsion Conference, Monterey (CA), 1989, paper AIAA 89-2861.

[14] D. G. Andrews, R. M. Zubrin, Magnetic sails and interstellar travel, Journal of The British Interplanetary Society 43 (6) (1990) 265–272 .

[15] R. M. Zubrin, D. G. Andrews, Magnetic sails and interplanetary travel, Journal of Spacecraft and Rockets 28 (2) (1991) 197–203, doi: 10.2514/3.26230.

[16] R. M. Zubrin, The use of magnetic sails to escape from low earth orbit, in: AIAA/SAE/ASME/ASEE 27th Joint Propulsion Conference, Sacramento (CA), 1991, paper AIAA 91-3352.

[17] R. M. Winglee, J. Slough, T. Ziemba, A. Goodson, Mini-magnetospheric plasma propulsion: Tapping the energy of the solar wind for spacecraft propulsion, Journal of Geophysical Research 105 (A9) (2000) 21,067–21,077 .

[18] G. Mengali, A. A. Quarta, Optimal missions with minimagnetospheric plasma propulsion, Journal of Guidance, Control, and Dynamics 29 (1) (2006) 209–212, doi: 10.2514/1.18169.

[19] G. Mengali, A. A. Quarta, Minimagnetospheric plasma propulsion for outer planet missions, Journal of Guidance, Control, and Dynamics 29 (5) (2006) 1239–1242, doi: 10.2514/1.21634.

[20] P. Janhunen, Electric sail for spacecraft propulsion, Journal of Propulsion and Power 20 (4) (2004) 763–764, doi: 10.2514/1.8580.

[21] G. Mengali, A. A. Quarta, P. Janhunen, Electric sail performance analysis, Journal of Spacecraft and Rockets 45 (1) (2008) 122–129, doi: 10.2514/1.31769.

[22] P. Janhunen, P. K. Toivanen, J. Polkko, S. Merikallio, P. Salminen, E. Haeggström, H. Seppänen, R. Kurppa, J. Ukkonen, S. Kiprich, G. Thornell, H. Kratz, L. Richter, O. Krömer, R. Rosta, M. Noorma, J. Envall, S. Lätt, G. Mengali, A. A. Quarta, H. Koivisto, O. Tarvainen, T. Kalvas, J. Kauppinen, A. Nuottajärvi, A. Obraztsov, Electric solar wind sail: Toward test missions, Review of Scientific Instruments 81 (11) (2010) 111301–1–11301–11, doi: 10.1063/1.3514548.

[23] P. Janhunen, Increased electric sail thrust through removal of trapped shielding electrons by orbit chaotisation due to spacecraft body, Annales Geophysicae 27 (8) (2009) 3089–3100, doi: 10.5194/angeo-27-3089-2009.

[24] J. Siguier, P. Sarrailh, J. Roussel, V. Inguimbert, G. Murat, J. SanMartin, Drifting plasma collection by a positive biased tether wire in LEO-like plasma conditions: current measurement and plasma diagnostics, IEEE Transactions on Plasma Science 41 (12) (2013) 3380–3386, doi: 10.1109/TPS.2013.2257871.

[25] P. Janhunen, Coulomb drag devices: electric solar wind sail propulsion and ionospheric deorbiting, Space Propulsion 2014, Köln, Germany, 2014, paper SP2014_2969331, Session 80.

[26] A. Kestilä, T. Tikka, P. Peitso, J. Rantanen, A. Näsilä, K. Nordling, H. Saari, R. Vainio, P. Janhunen, J. Praks, M. Hallikainen, Aalto-1 nanosatellite – technical description and mission objectives, Geoscientific Instrumentation, Methods and Data Systems 2 (2013) 121–130, doi: 10.5194/gi-2-121-2013.

[27] O. Khurshid, T. Tikka, J. Praks, M. Hallikainen, Accommodating the plasma brake experiment on-board the aalto-1 satellite, Proceedings of the Estonian Academy of Sciences 63 (2S) (2014) 258–266, doi: 10.3176/proc.2014.2S.07.

[28] M. Y. Huo, F. J. Peng, J. Zhao, S. B. Xie, N. M. Qi, Trajectory optimization for ceres exploration with an electric sail, Journal of Astronautics 36 (12) (2015) 1363–1372 .

[29] A. Sanchez-Torres, Propulsive force in an electric solar sail for outer planet missions, IEEE Transactions on Plasma Science 43 (9) (2015) 3130–3135, doi: 10.1109/TPS.2015.2431649.

[30] P. Janhunen, S. Merikallio, M. Paton, EMMI - electric solar wind sail facilitated manned mars initiative, Acta Astronautica 113 (2015) 22–28, doi: 10.1016/j.actaastro.2015.03.029.

[31] G. Mengali, A. A. Quarta, G. Aliasi, A graphical approach to electric sail mission design with radial thrust, Acta Astronautica 82 (2) (2013) 197–208, doi: 10.1016/j.actaastro.2012.03.022.

[32] K. Yamaguchi, H. Yamakawa, Electric solar wind sail kinetic energy impactor for near earth asteroid deflection mission, In press. The Journal of the Astronautical Sciences .

[33] K. Yamaguchi, H. Yamakawa, Study on orbital maneuvers for electric sail with on-off thrust control, Aerospace Technology Japan 12 (2013) 79–88, doi: 10.2322/astj.12.79.

[34] P. Janhunen, A. Sandroos, Simulation study of solar wind push on a charged wire: basis of solar wind electric sail propulsion, Annales Geophysicae 25 (3) (2007) 755–767, doi: 10.5194/angeo-25-755-2007.

[35] A. A. Quarta, G. Mengali, Analysis of electric sail heliocentric motion under radial thrust, In press. Journal of Guidance, Control and Dynamicsdoi: 10.2514/1.G001632.

[36] P. Janhunen, The electric solar wind sail status report, in: European Planetary Science Congress 2010, Vol. 5, European Planetology Network and the European Geosciences Union, 2010, paper EPSC 2010-297.

[37] A. A. Quarta, G. Mengali, Trajectory approximation for low-performance electric sail with constant thrust angle, Journal of Guidance, Control, and Dynamics 36 (3) (2013) 884–887, doi: 10.2514/1.59076.

[38] G. Mengali, A. A. Quarta, Non-keplerian orbits for electric sails, Celestial Mechanics and Dynamical Astronomy 105 (1–3) (2009) 179–195, doi: 10.1007/s10569-009-9200-y.

[39] A. A. Quarta, G. Mengali, Electric sail mission analysis for outer solar system exploration, Journal of Guidance, Control, and Dynamics 33 (3) (2010) 740–755, doi: 10.2514/1.47006.

[40] G. Aliasi, G. Mengali, A. A. Quarta, Artificial equilibrium points for an electric sail with constant attitude, Journal of Spacecraft and Rockets 50 (6) (2013) 1295–1298, doi: 10.2514/1.A32540.

[41] L. Niccolai, A. A. Quarta, G. Mengali, Refined analysis of electric sail-based displaced orbits, in: 5th International Conference on Tethers in Space, Ann Arbor, Michigan (USA), 2016.

[42] A. A. Quarta, G. Mengali, P. Janhunen, Optimal interplanetary rendezvous combining electric sail and high thrust propulsion system, Acta Astronautica 68 (5-6) (2011) 603–621, doi: 10.1016/j.actaastro.2010.01.024.

[43] G. Mengali, A. A. Quarta, Optimal nodal flyby with near-earth asteroids using electric sail, Acta Astronautica 104 (2) (2014) 450–457, doi: 10.1016/j.actaastro.2014.02.012.

[44] D. F. Lawden, Optimal Trajectories for Space Navigation, Butterworths, London, 1963, pp. 54–68.

[45] G. E. Forsythe, A. M. Michael, C. B. Moler, Computer Methods for Mathematical Computations, Prentice-Hall, Englewood Cliffs, NJ, 1977, pp. 192–235, ISBN: 978-0131653320.

[46] A. E. Bryson, Y. C. Ho, Applied Optimal Control, Hemisphere Publishing Corporation, New York, NY, 1975, Ch. 2, pp. 71–89, ISBN: 0-891-16228-3.

[47] P. Janhunen, A. A. Quarta, G. Mengali, Electric solar wind sail mass budget model, Geoscientific Instrumentation, Methods and Data Systems 2 (1) (2013) 85–95, doi: 10.5194/gi-2-85-2013.

List of Tables

i	0	1	2	3	4	5	6
b_i	0	4.853×10^{-1}	3.652×10^{-3}	-2.661×10^{-4}	6.322×10^{-6}	-8.295×10^{-8}	3.681×10^{-10}
c_i	1.000	6.904×10^{-5}	-1.271×10^{-4}	7.027×10^{-7}	-1.261×10^{-8}	1.943×10^{-10}	-5.896×10^{-13}

Table 1
Best-fit interpolation coefficients of thrust parameters (angles α and α_n in degrees). Data adapted from Ref. [33].

List of Figures

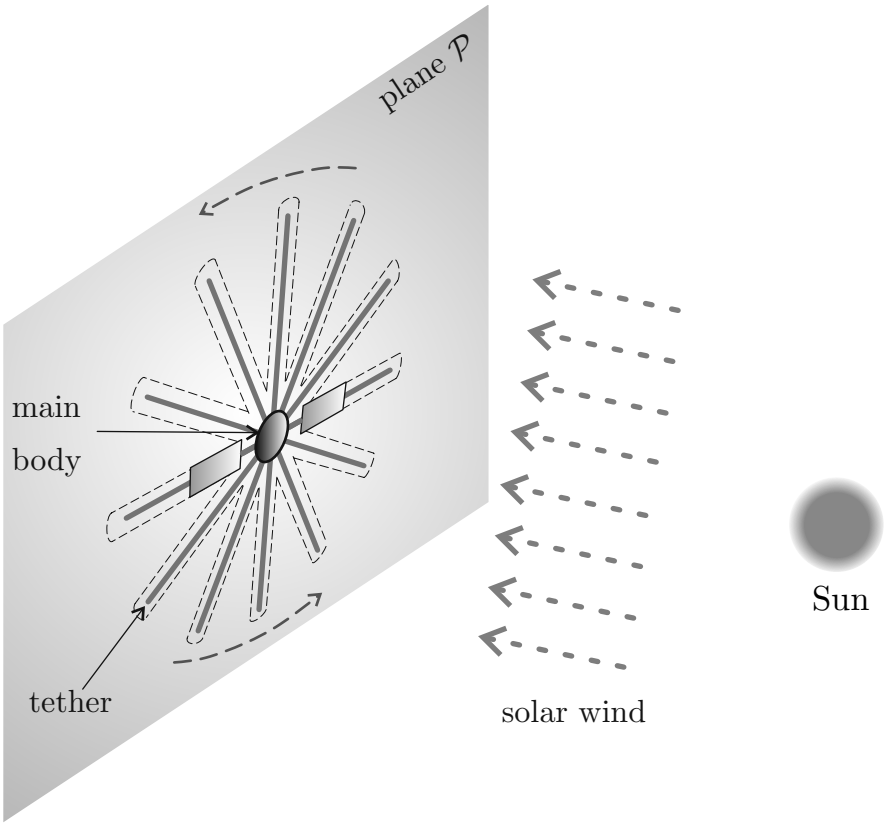

Figure 1. E-sail conceptual scheme.

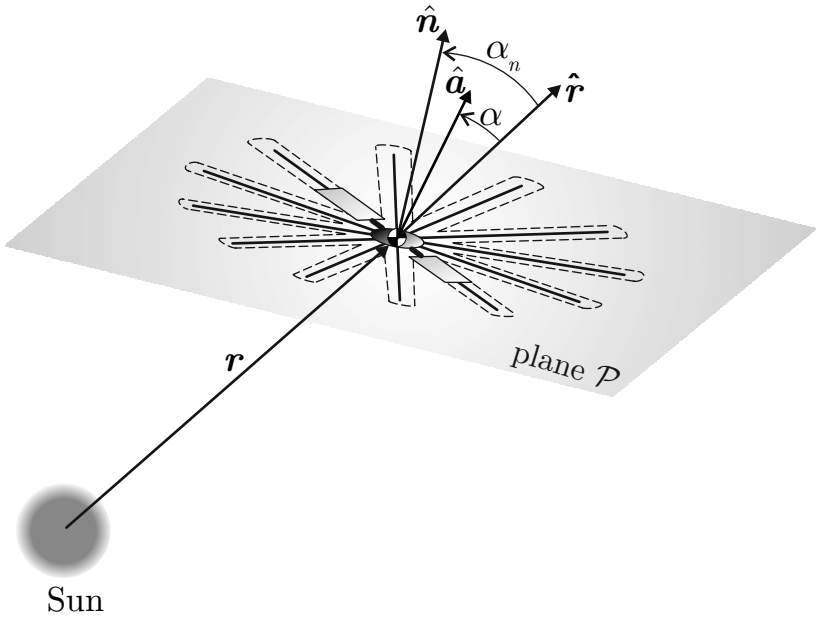

Figure 2. E-sail cone (α) and pitch (α_n) angle.

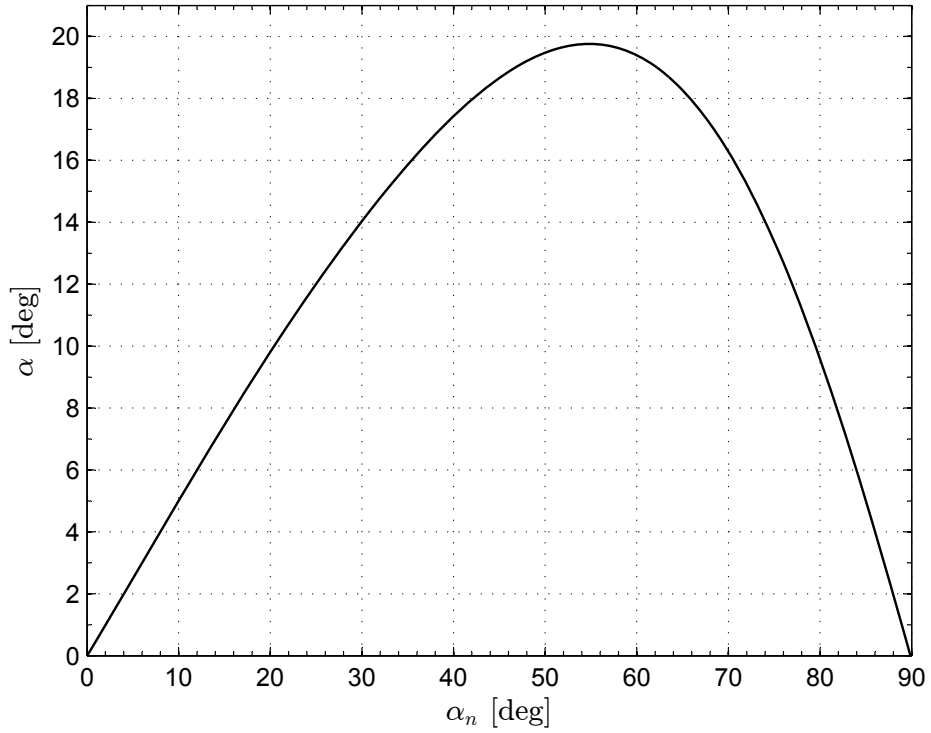

(a) Cone angle.

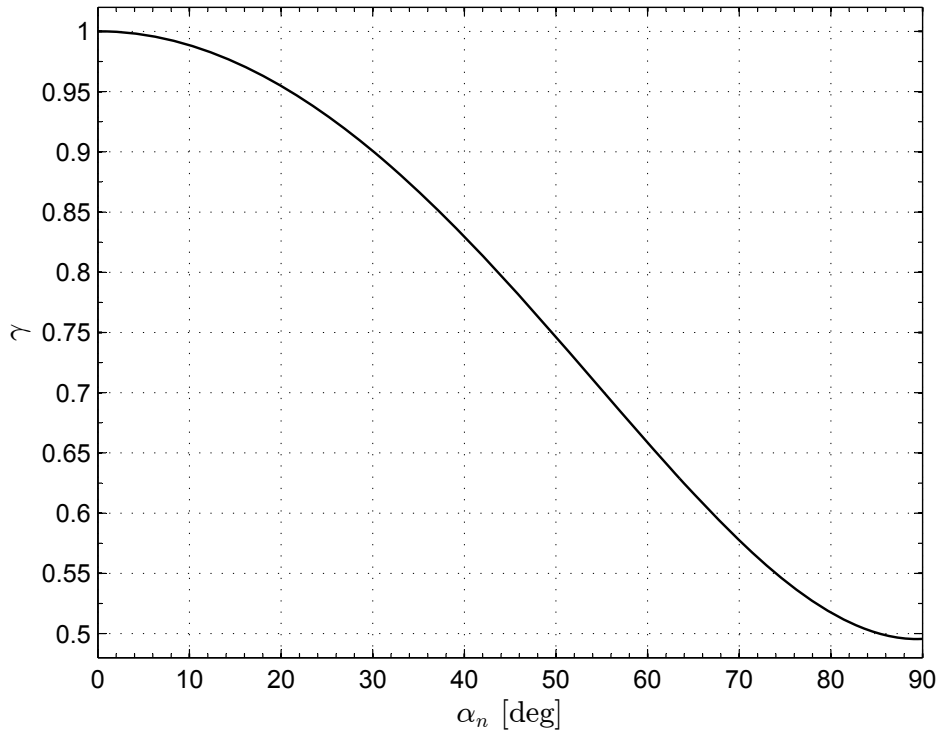

(b) Dimensionless propulsive acceleration.

Figure 3. Cone angle and dimensionless propulsive acceleration as a function of pitch angle α_n. Data adapted from Ref. [33].

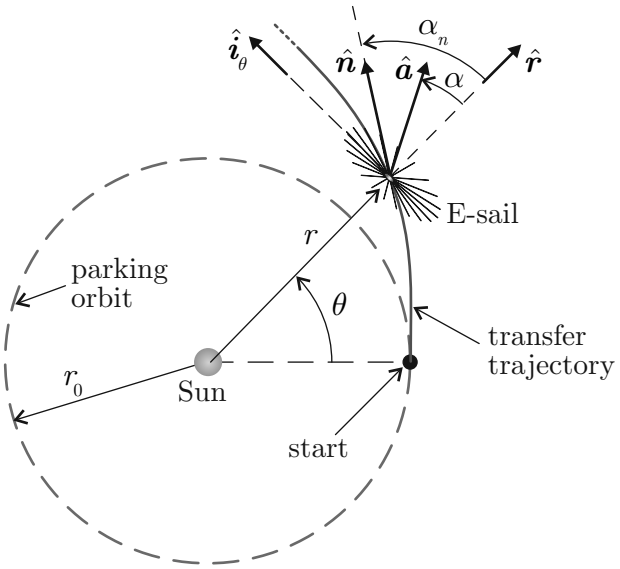

Figure 4. Reference frame and characteristic angles.

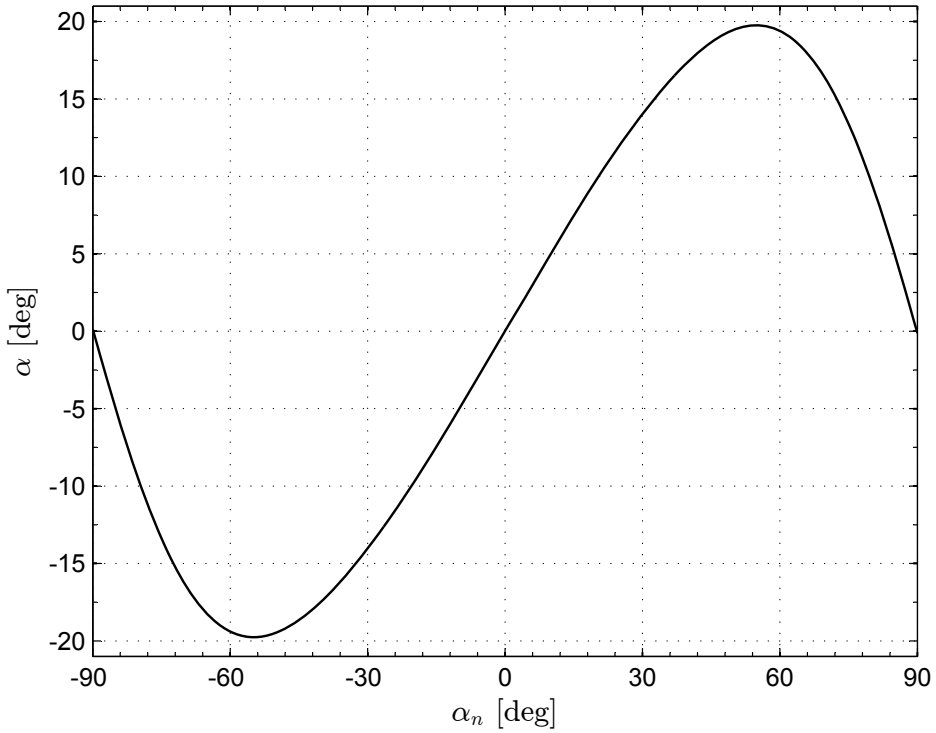

(a) Cone angle.

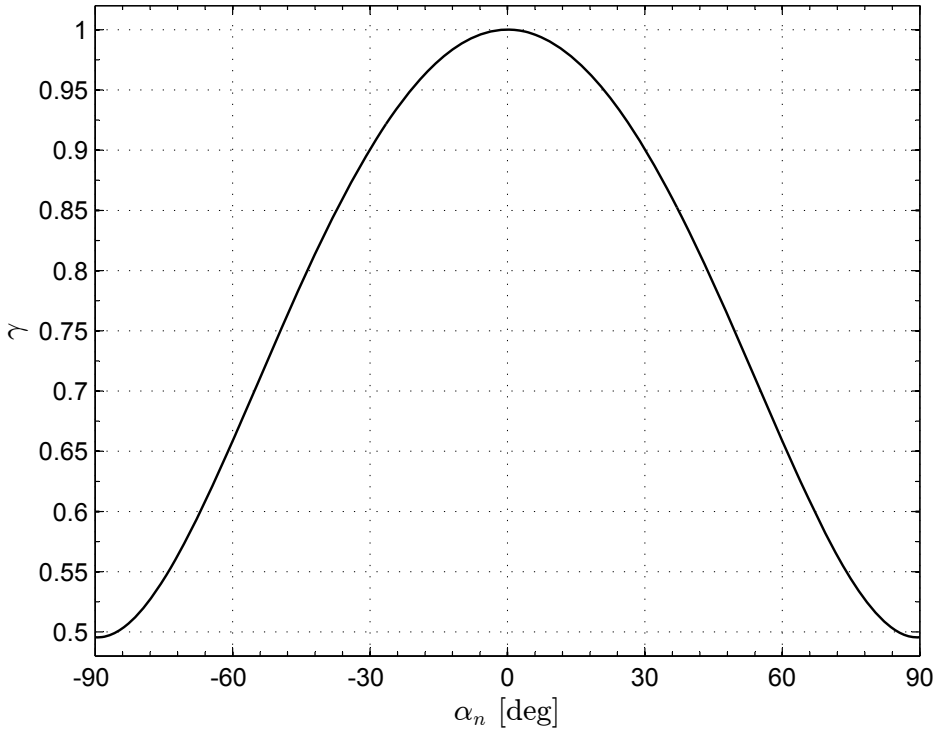

(b) Dimensionless propulsive acceleration.

Figure 5. E-sail propulsive characteristics for mission analysis purposes in a two-dimensional scenario.

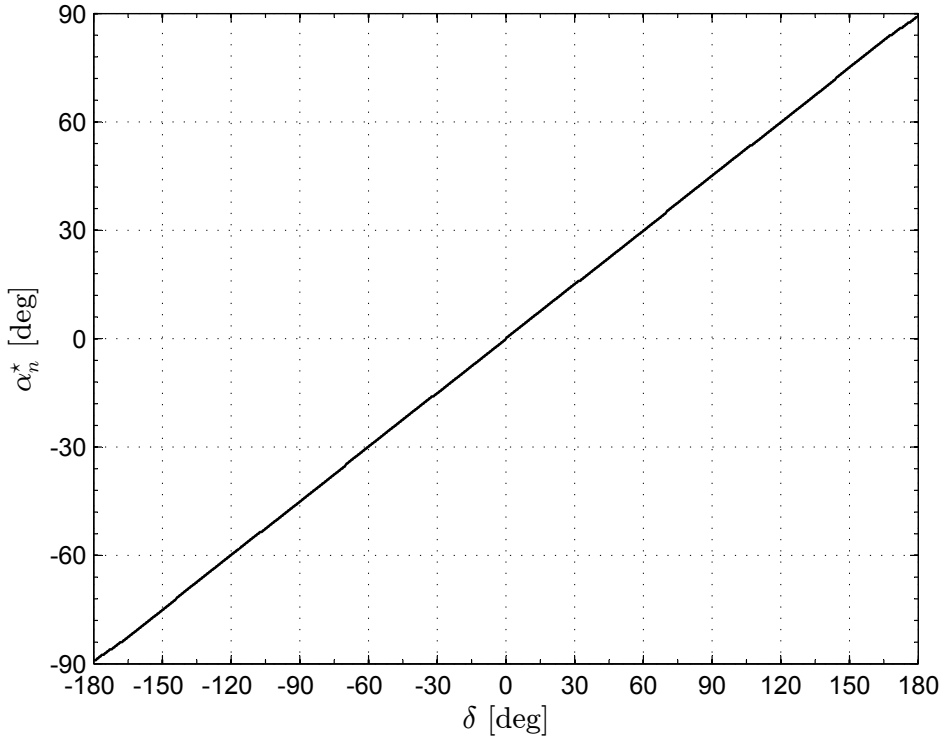

(a) Optimal pitch angle.

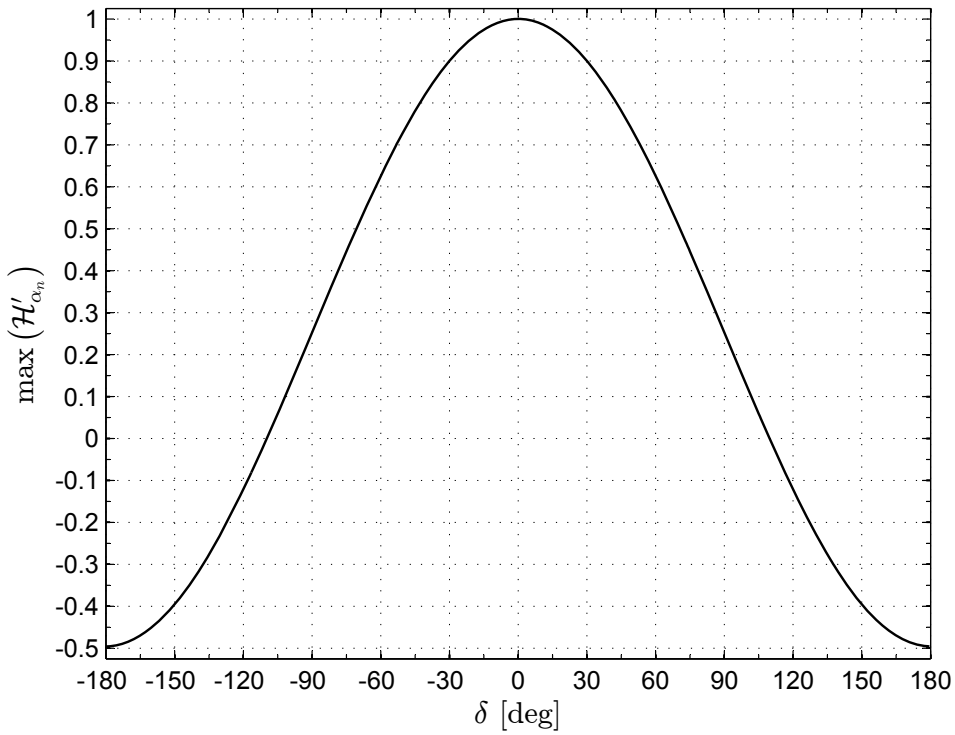

(b) Maximum value of $\mathcal{H}'_{\alpha_n}$.

Figure 6. Optimal value of pitch angle and maximum of the reduced Hamiltonian as a function of δ.

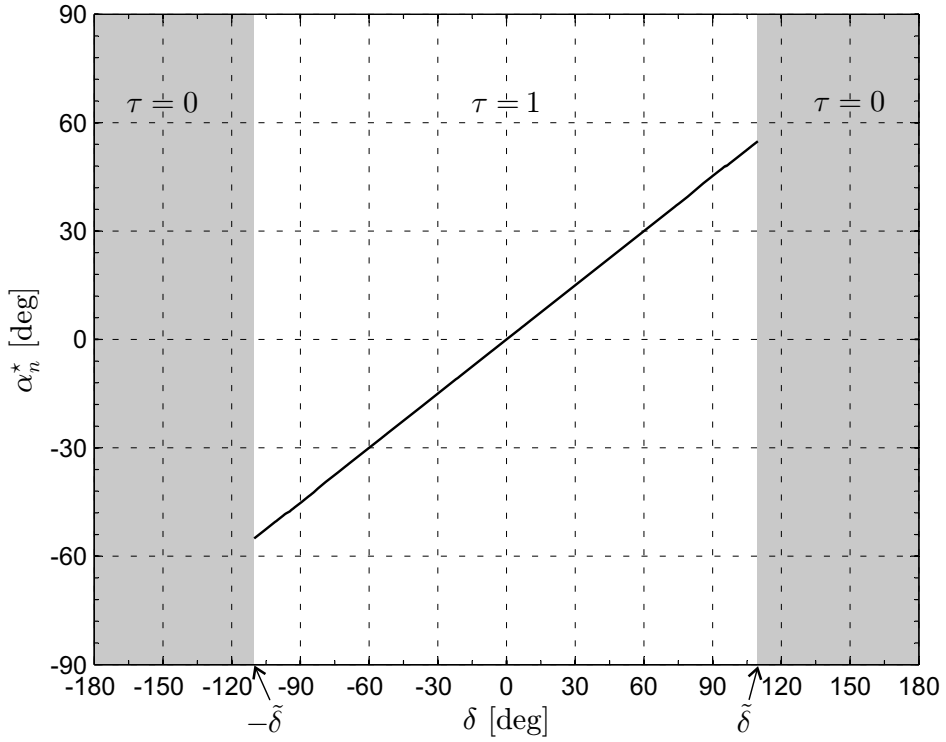

Figure 7. Optimal control law as a function of the primer vector's cone angle δ.

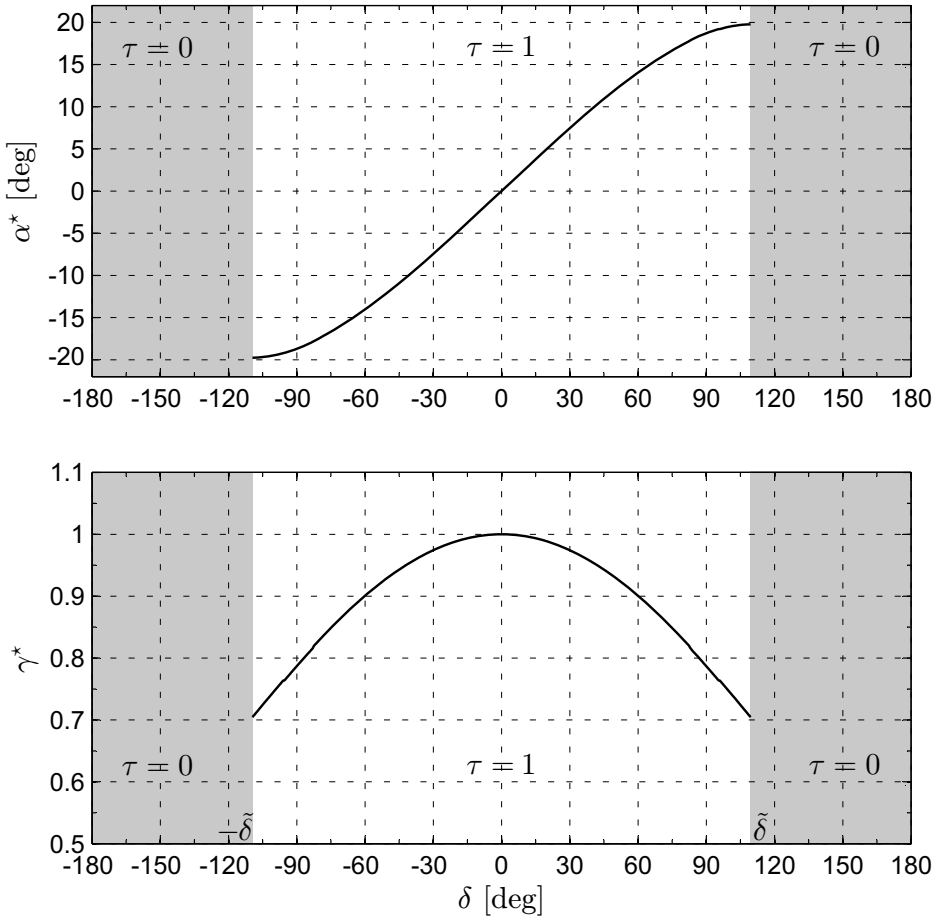

Figure 8. Optimal cone angle and dimensionless propulsive acceleration of δ.

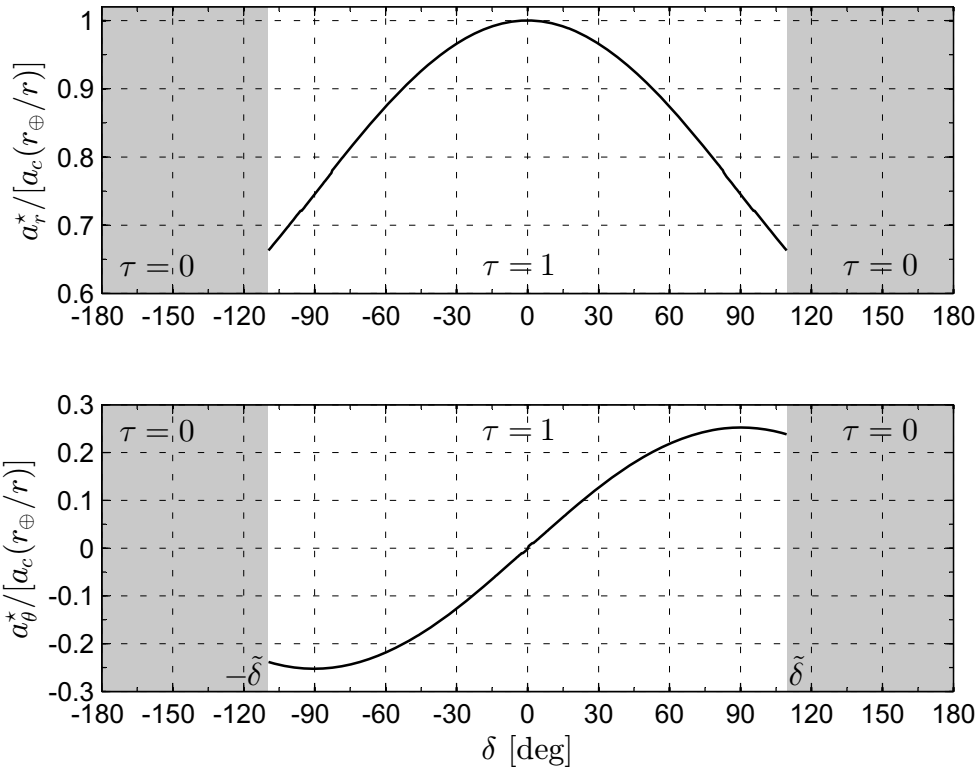

Figure 9. Optimal dimensionless components of the propulsive acceleration as a function of δ.

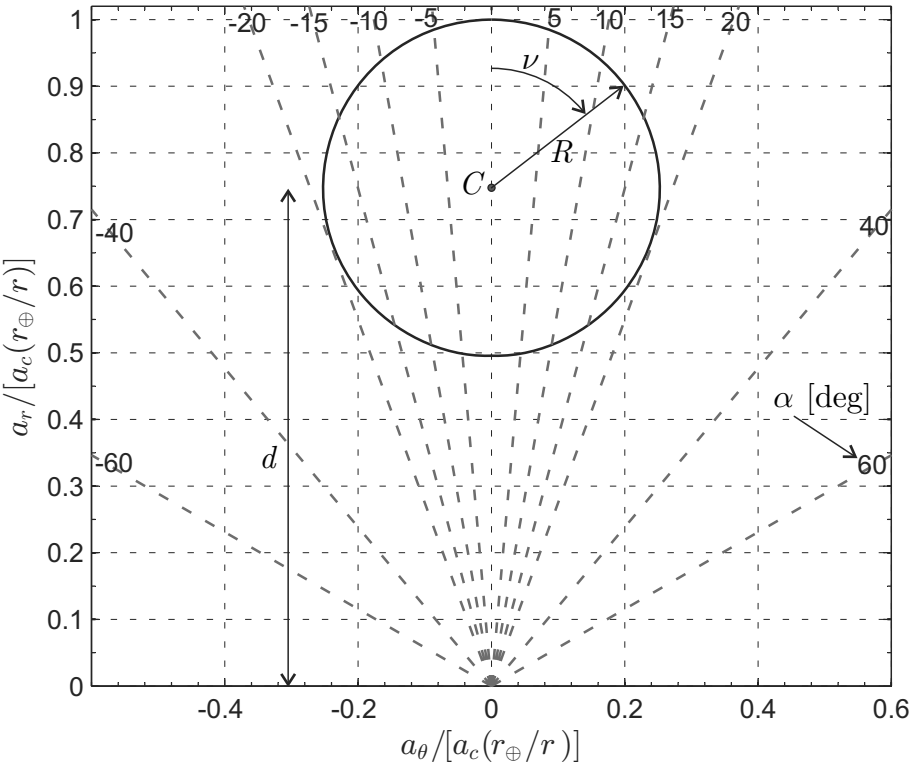

Figure 10. Components of the dimensionless propulsive acceleration.

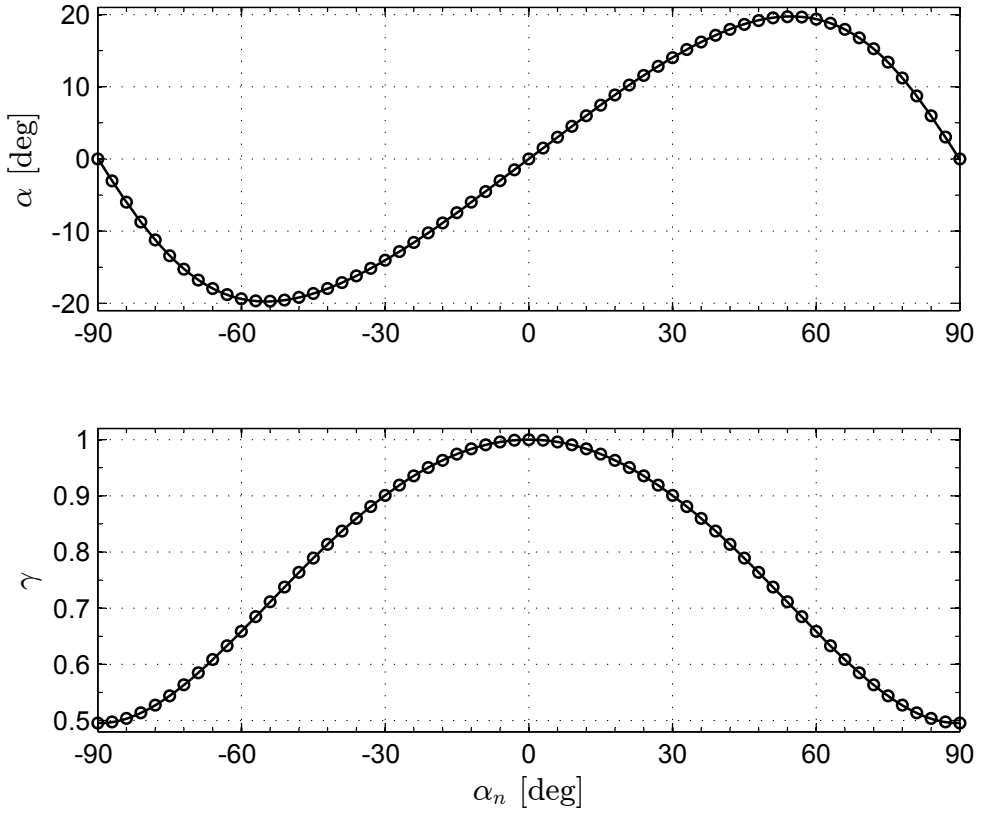

Figure 11. Cone angle and dimensionless propulsive acceleration as a function of the pitch angle: best–fit polynomial [solid line, see Eqs. (9)-(10)] vs. analytical approximation [circles, see Eqs. (34)-(35)].

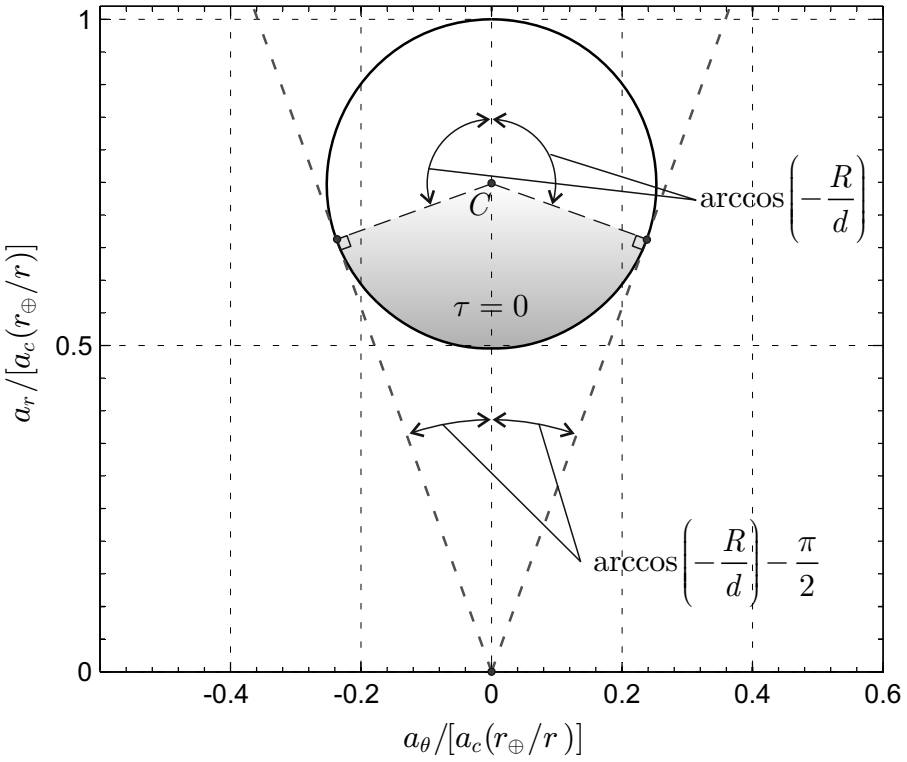

Figure 12. Thruster-off condition in the (a_θ, a_r) plane, see Eq. (41).

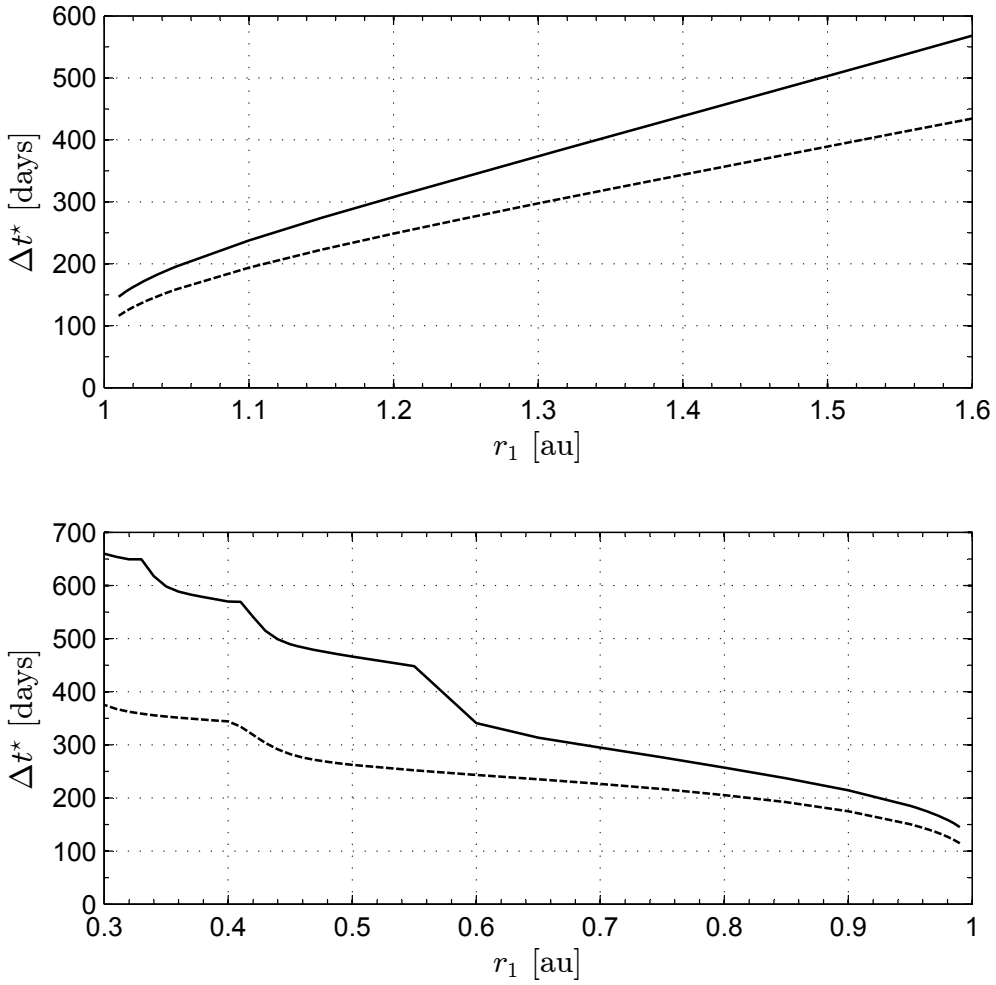

Figure 13. Minimum transfer time as a function of the final radius. Refined (solid line) vs. classical (dashed line) thrust model, see Eq. (3).

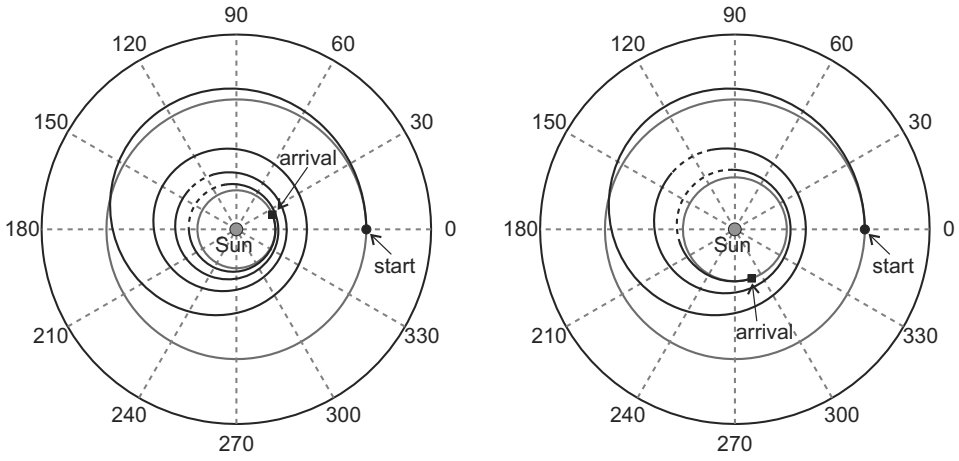

(a) $r_1 = 0.3\,\text{au}$.

(b) $r_1 = 0.4\,\text{au}$.

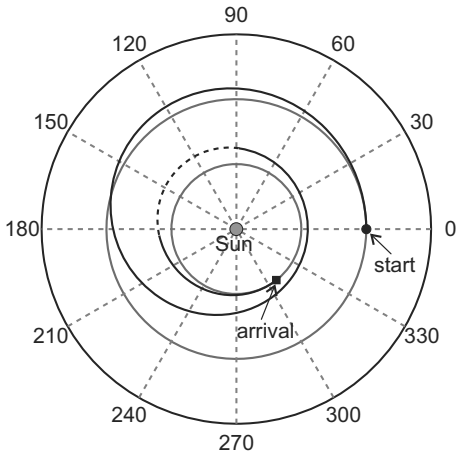

(c) $r_1 = 0.5\,\text{au}$.

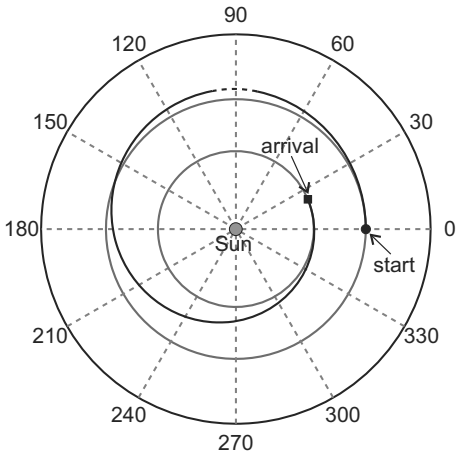

(d) $r_1 = 0.6\,\text{au}$.

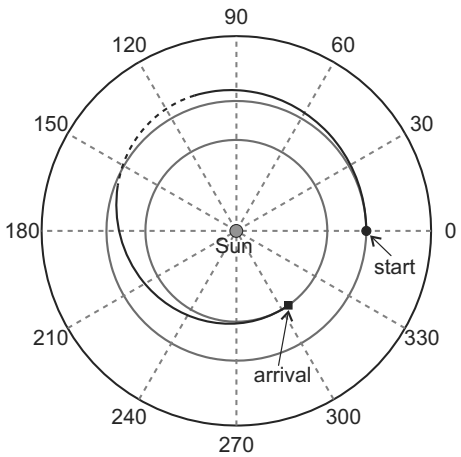

(e) $r_1 = 0.7\,\text{au}$.

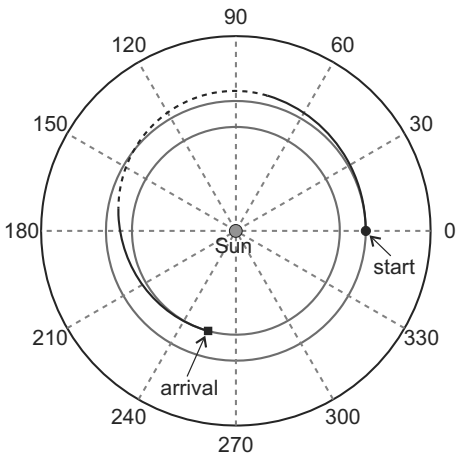

(f) $r_1 = 0.8\,\text{au}$.

Figure 14. Optimal circle-to-circle transfer trajectories as a function of the final radius r_1 when $r_0 = 1\,\text{au}$ and $a_c = 1\text{mm/s}^2$. Dashed lines correspond to coasting arcs.

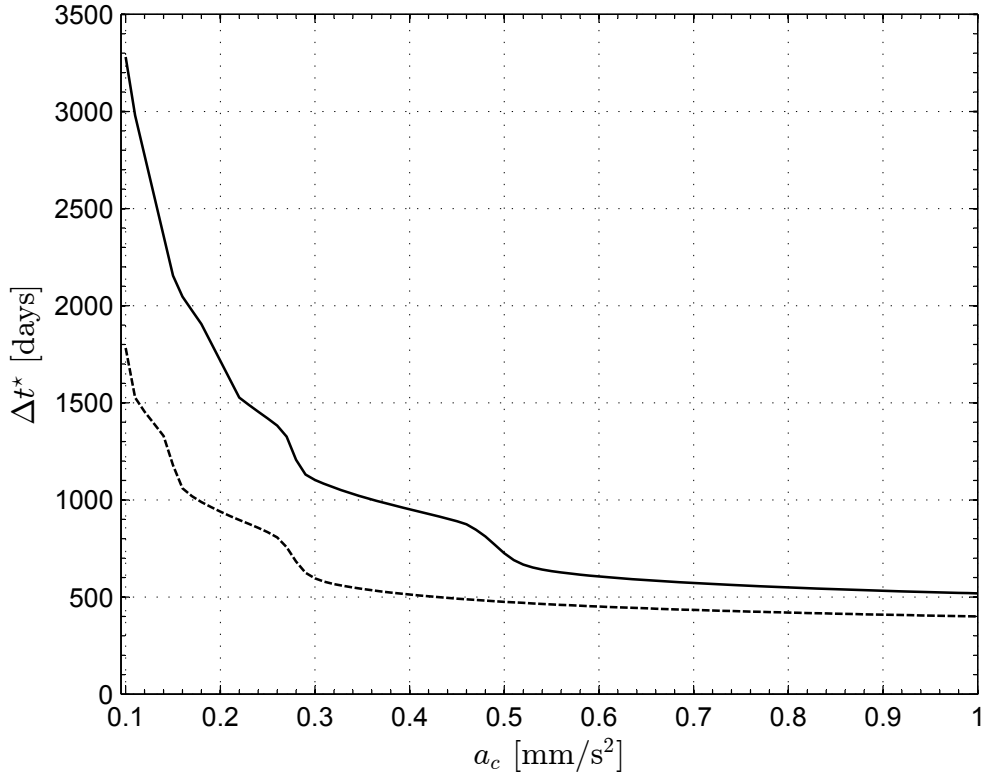

Figure 15. Minimum transfer time as a function of a_c in a simplified, circle-to-circle, Earth-Mars mission scenario. Refined (solid line) vs. classical (dashed line) thrust model, see Eq. (3).

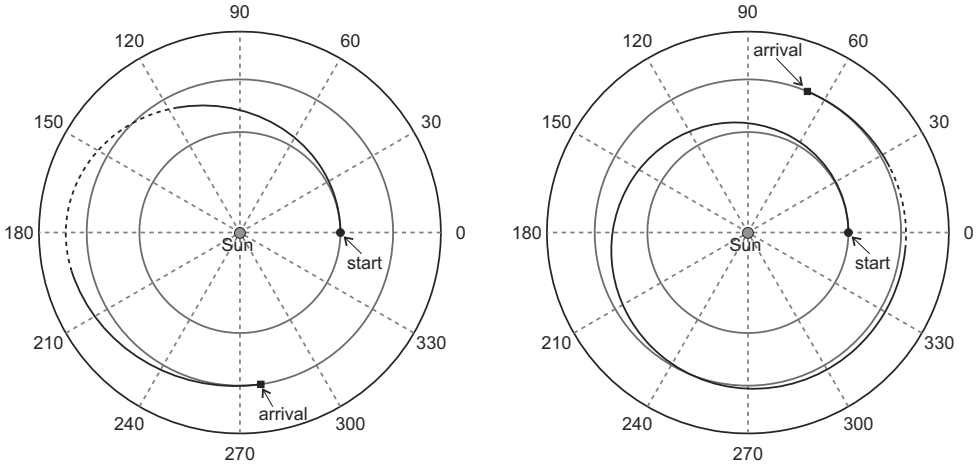

(a) $a_c = 1\,\mathrm{mm/s^2}$. (b) $a_c = 0.5\,\mathrm{mm/s^2}$.

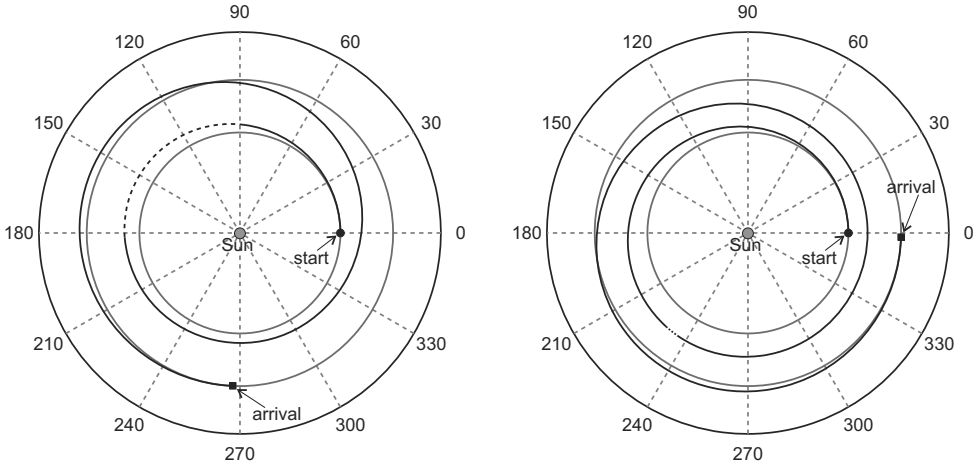

(c) $a_c = 0.4\,\mathrm{mm/s^2}$. (d) $a_c = 0.3\,\mathrm{mm/s^2}$.

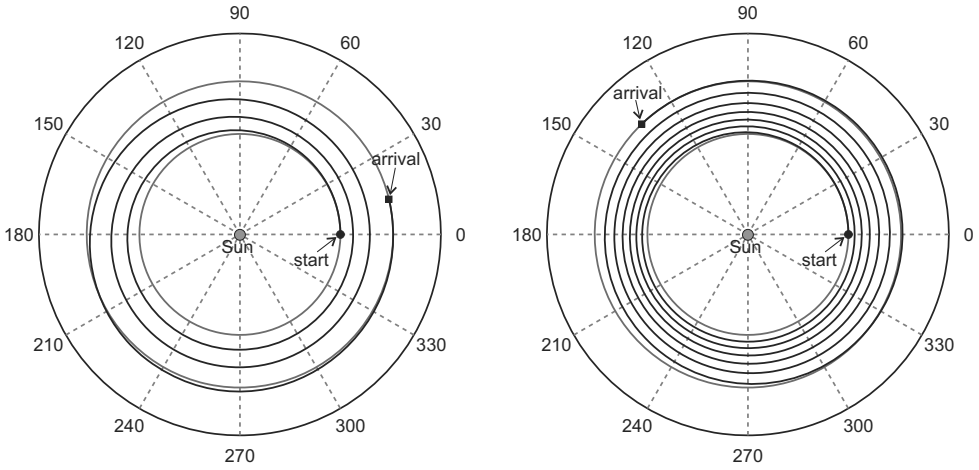

(e) $a_c = 0.2\,\mathrm{mm/s^2}$. (f) $a_c = 0.1\,\mathrm{mm/s^2}$.

Figure 16. Optimal Earth-Mars circle-to-circle transfer trajectories as a function of the characteristic acceleration. Dashed lines correspond to coasting arcs.

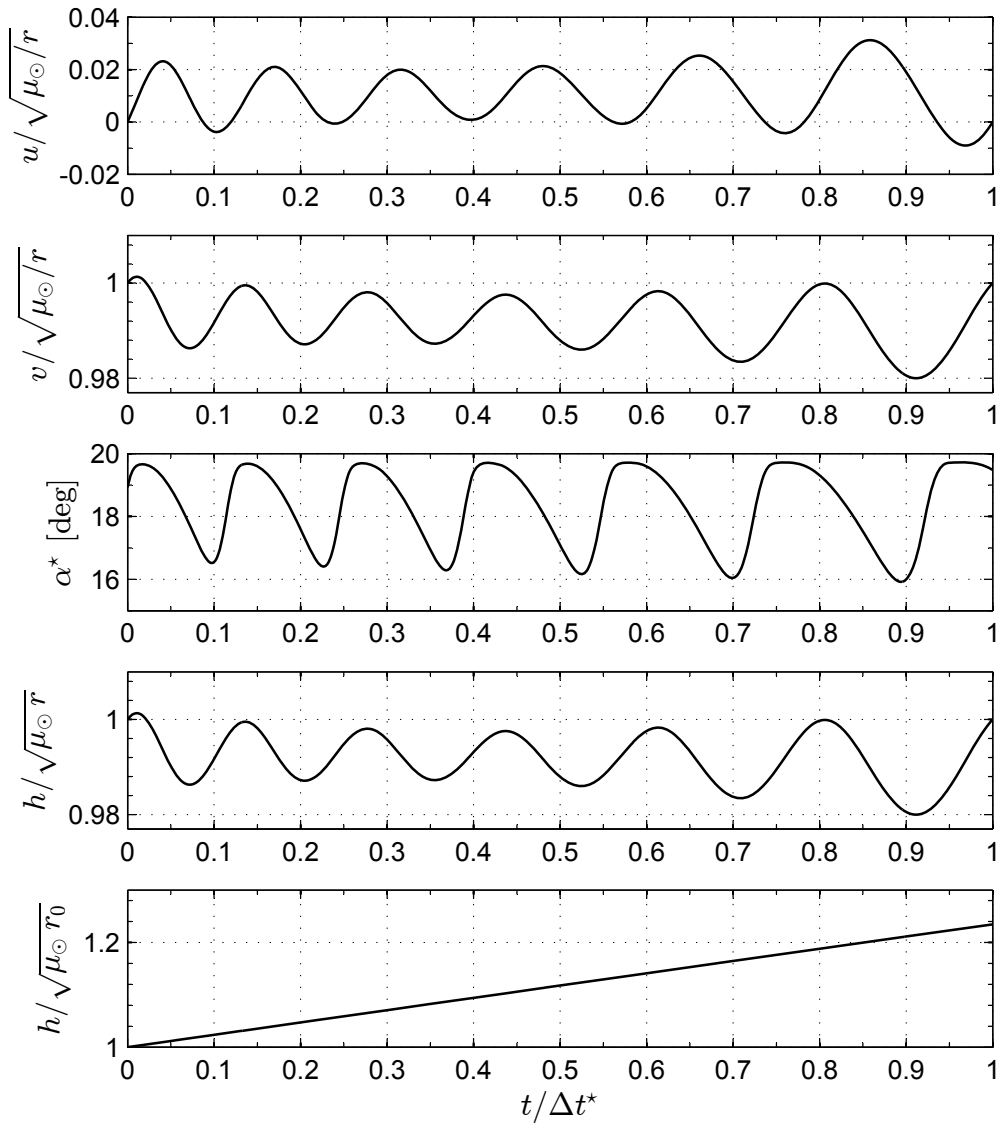

Figure 17. Results for an Earth-Mars circle-to-circle optimal transfer with a refined thrust model ($\Delta t^\star \simeq 3281$ days).

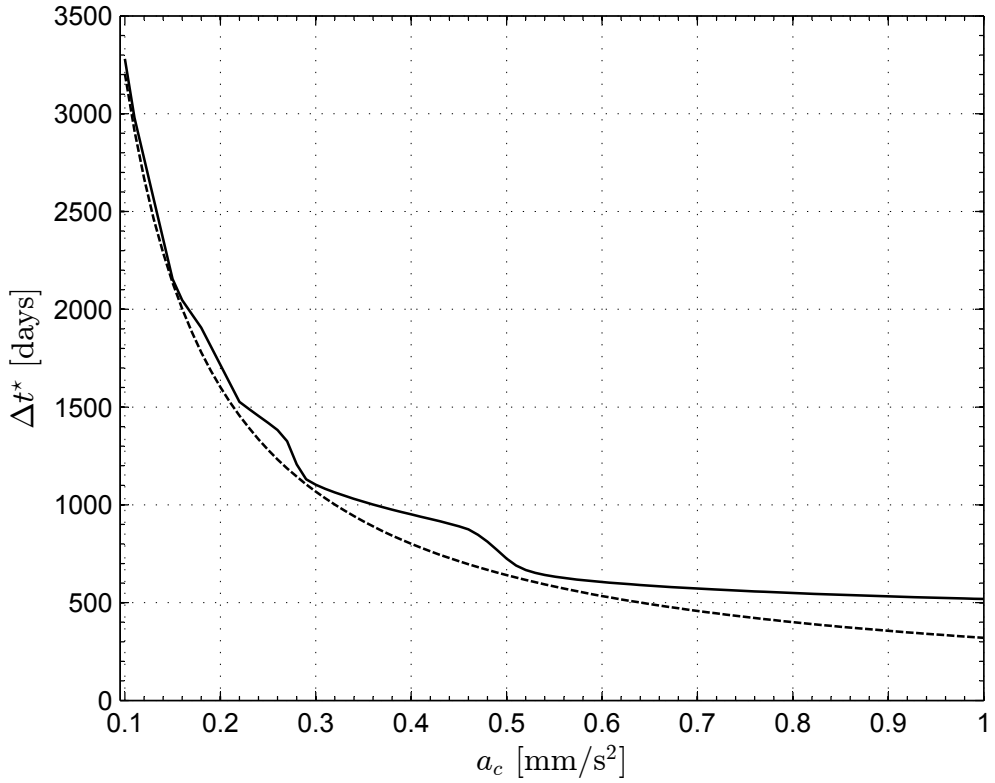

Figure 18. Earth-Mars optimal circle-to-circle transfer. Comparison between actual flight time (solid line) and approximated value from Eq. (49) (dashed line).